Neutrino Flavour Conversions in a Supernova Shock-wave

A thesis submitted to the
Tata Institute of Fundamental Research, Mumbai
for the degree of
Master of Science, in Physics

by
Basudeb Dasgupta
Department of Theoretical Physics, School of Natural Sciences
Tata Institute of Fundamental Research, Mumbai
July, 2006

I dedicate this thesis to my loving parents

Acknowledgements

I would like to gratefully acknowledge the guidance and support that I have recieved from Amol Dighe, my thesis advisor, over the last two years. No words of gratitude will ever convey my regard for him.

The faculty at TIFR have been very helpful and friendly. I thank my professors, in particular Amol, Kedar, Shiraz and Sunil for very enjoyable and exciting lectures.

Thanks are also due to the DTP office staff for their help and unsurpassable efficiency in sorting out every trouble I took to them.

I acknowledge the financial support recieved from Max Planck India Partner Group and the TIFR Endowment Fund.

I also wish to take this opportunity to convey my love and regards for my parents and brother. Whenever I have needed them, I have always found them by my side. My thanks also to my friends here and elsewhere, for their wonderful company.

Finally, I would like to express my gratitude to my teachers from Jadavpur University who gave me the inspiration to study physics.

Synopsis

Neutrino oscillation is now a well established phenomenon in Nature. There are interesting issues in physics and astrophysics that are addressed using the framework of neutrino oscillations. Some outstanding problems like the atmospheric and solar neutrino deficit have now been understood elegantly in terms of flavour conversions of massive neutrinos. While the paradigm of massive neutrinos is part of the standard picture now, precision measurement of mass and mixing parameters is not yet complete. In particular, we still only have an upper-bound of 13° on the mixing angle θ_{13}. A careful and precise measurement of all such parameters is imperative, if we want to discriminate between various possible extensions to the Standard Model. This is the general and driving motivation for studying the physics of neutrinos.

In this thesis we focus our attention to effects of ambient matter on neutrinos propagating through it. This is an important aspect and needs careful consideration, because naive expectations ignoring matter-effects can be way off-mark, typically when a critical density of matter (called a resonance) is encountered. We discuss different techniques used to calculate the matter-effect induced enhancement in the survival probability $P(\nu_e \to \nu_e)$ of neutrinos travelling through matter of generically varying density in a two and three neutrino framework. There exist exact analytical expressions for $P(\nu_e \to \nu_e)$ only for a few simple cases and useful approximations for situations with monotonically varying density. However, in literature there are no solutions for a medium with a general non-monotonic density profile. We present a new method to calculate $P(\nu_e \to \nu_e)$ approximately for the cases where the density of the medium may vary non-monotonically. We show that our solution is in excellent agreement with an exact numerical solution, in the region of its validity. It is seen that there exists in general, a novel effect that is present in such a situation. The physical basis of the effect is that, neutrinos of different energies acquire a different quantum-phase as they propagate

between successive resonances encountered in the non-monotonic profile. This phase enters the survival probability and therefore manifests itself as an energy dependent oscillatory modulation of the flux of neutrinos. These wiggles in the energy spectrum are shown to be intimately connected to the form of the density profile of the medium. This effect was ignored in previous works which calculated the survival probability, based on the assumption that the neutrino wave-packets decohere completely on their journey between successive resonances.

In addition we discuss the consequences of the above analyses for neutrinos coming from supernovae. We show that there is a signature generated in the observed neutrino spectrum, when the neutrinos pass through the non-monotonic density profile of an exploding supernova, due to the effect mentioned earlier. We take a typical density profile from a current simulation and numerically calculate the survival probability of neutrinos as it propagates through it. We take typical models of neutrino fluxes and show that the signature is robust and independent of the model chosen for fluxes. We investigate the possibility of experimental observation of the above mentioned signature. We find that if the value of θ_{13} is such that the resonances that are encountered are semi-adiabatic, these phase effects may be significant. This typically happens for θ_{13} of about a few degrees. Some constraints on mass and mixing parameters can be put from the observation of these effects. Specifically one may be able to put a lower-bound on the value of θ_{13} and determine the mass-hierarchy. We also show that it is possible to extract information about the supernova shock-wave profile behind the reverse-shock from the neutrino spectrum if the observation is possible. However, we find that using present and planned detectors, such an observations is unlikely, unless the supernova explosion occurs about a kilo-parsec away. This undermines to some extent the experimental significance of the novel phase effects that we point out.

Contents

Chapter 1

Introduction

Our present understanding of the microscopic laws of nature is governed by the Standard Model (SM) of particle physics. It is a gauge theory based on the group $SU(3)_C \times SU(2)_L \times U(1)_Y$. Matter is classified into three generations, with each generation comprising of an up-type quark ($u,\ c,\ t$), a down-type quark ($d,\ s,\ b$), a charged lepton ($e,\ \mu,\ \tau$), and a neutral lepton called neutrino ($\nu_e,\ \nu_\mu,\ \nu_\tau$). These particles interact with each other via the strong, weak and electromagnetic forces which are mediated by the respective gauge bosons. The eight gluons (G) of $SU(3)_C$ mediate the strong force. Of the four bosons of $SU(2)_L \times U(1)_Y$, two (W^+, W^-) mediate the weak charged current interactions . One linear combination of the remaining two (Z) mediates the weak neutral current interactions, and the other is the photon (γ) that mediates electromagnetism. There is additionally a scalar boson in the theory, known as the Higgs, which has not been observed yet.

Matter in SM is best described by bispinor fermion solutions to the Dirac equation. They contain both the particle and antiparticle degrees of freedom, each of which can be resolved into their left and right-chiral components. These left and right-handed components of the fermion and the Higgs scalar interact at a vertex through a Yukawa coupling. When the Higgs scalar gets a vacuum expectation value via spontaneous symmetry breaking it introduces a mass term for the fermion. As it stands, SM does not have mass terms for neutrinos due to the absence of right-handed neutrinos. This model is immensely successful

and explains most of the experimental data accurately. A few experimental results in neutrino physics are difficult to explain in the above framework. The classic examples being the atmospheric and solar neutrino problems [1, 2]. They essentially point out the fact that the flux of neutrinos detected from a known source turns out to be different from what is expected on the basis of SM and existing models of the source fluxes. There are two kinds of solutions to these problems, astrophysical and physical. The astrophysical solutions are based on the approach that our understanding of the source fluxes is not satisfactory and therefore propose to modify either the model of the source and/or the medium, through which neutrinos travel, to account for the disagreement. This requires addressing each physical situation independently, which is clearly not a minimal approach. The physical solutions act at a more fundamental level, and explain the discrepancy by making changes to the properties of neutrinos and/or their interactions, which modify our expectation for the fluxes. This approach allows all the neutrino problems to be addressed together. There were various suggestions that belonged to the latter category, but the paradigm of neutrinos with tiny masses, explains all the available data and seems to be the most favoured solution. There exist models that extend the SM to include massive neutrinos [3].

In the quark sector we are familiar with the notion that the up-type quark mass matrix and the down-type quark mass matrix are not simultaneously diagonalised. This causes the different generations of quarks to mix via what is known as the Cabbibo-Kobayashi-Masakawa (CKM) matrix [4, 5]. For massive neutrinos, this possibility is realised in the lepton sector too. There is a misalignment of the charged lepton mass matrix and the neutrino mass matrix. The charged lepton weak interaction eigenstates are by convention taken as the same as the mass eigenstates and the neutrino weak interaction eigenstates are then related to their mass eigenstates by a unitary transformation parametrised by the Pontecorvo-Maki-Nakagawa-Sakata (PMNS) matrix [6, 7]. This allows for neutrinos of one flavour to convert into another and gives rise to lepton flavour oscillation [6] exactly like strangeness oscillations. When one considers propagation of neutrinos through matter, the rate of flavor conversion depends crucially on the electron density (and its gradient) in the ambient matter [8]. This is

referred to as matter effects and we will investigate this aspect in some detail. In particular we will see that the rate of conversion of one flavour to another can suddenly become very large at a certain value of the density of the medium [9, 10]. A sharp change in the density also enhances neutrino conversion [11]. All these effects need to be taken into account when calculating the expected flux of neutrinos from a given source. This is what goes into the resolution of the solar and atmospheric neutrino problems.

These phenomena depend quantitatively on the neutrino masses and the mixing matrix. So it is important that we make a precise measurement of the relevant parameters. That will not only provide us a detailed explanation to the said neutrino deficit problems, but also serve as a useful guide to what kind of extensions one should expect beyond SM. This follows from the fact that the wide variety of models naturally prefer different values for the mass and mixing parameters, and if we can experimentally measure some of the discriminatory parameters, models naturally predicting the observed parameter values will be favoured over others. The object of this thesis is to explore the paradigm of neutrino oscillations with particular emphasis to matter effects. The reason matter effects are being emphasised is that some mixing parameters are probed efficiently in the presence of such effects, e.g. the case of neutrinos coming from supernovae, or neutrinos travelling through the earth matter. Conversely, if the neutrino parameters are well measured, then these effects can be used to probe the density variation of the media.

These problems are extremely exciting and a subject of active research. We will confine ourselves to provide only as much detail as is required to be able to introduce and analyse the new results that we present in this thesis, i.e. the idea of phase effects. A lot of the material presented in this thesis draws from standard textbooks, reviews and papers. Some of the introductory material is "inspired" from the lectures by Dighe [12]. We mention below some references that are relevant to various aspects of this thesis. A detailed description of how we were led to a consistent and unified picture of neutrino oscillations, issues about nature of neutrino masses, neutrino mass models and related phenomenology can be found in the following textbooks [13, 14]. Pedagogical treatments of neutrino oscillations can be found in the following review [15]. Matter effects are discussed

in great detail in this review [17]. SN neutrinos are discussed in these reviews [18, 19]. The treatment of effects of the shock-wave(s) on neutrinos is presented in these papers [16, 20, 21, 22]. Phase effects are discussed in our paper [23].

1.1 Neutrinos in physics

We begin by tracing out the history of neutrinos to understand the role that they have played in our understanding of particle physics, to provide a motivation to study neutrinos and to acquire the required background for the later chapters.

1.1.1 The Pauli hypothesis

Beta decays were thought to be two-body decays because only the electron and the daughter nucleus were observed. A two-body decay should result in a fixed electron energy. However, the electron energy was seen to be continuous. Either the conservation of energy and momentum was in peril, or something was missing. Pauli proposed in 1932 that the decay was a three-body decay and a chargeless and massless particle, termed "neutrino" was being emitted and not being observed. The introduction of neutrinos not only took care of the energy-momentum conservation, it also explained the shape of the electron spectrum observed. These experiments put an upper bound on the neutrino mass, e.g. the tritium decay experiment at Mainz gives an upper bound on the mass of the neutrino with mostly electron component to be 2.3 eV [24]. Bounds on other flavours from similar experiments are large, but successful nucleosynthesis after the Big Bang requires the sum of all neutrino masses to be less than about 0.68 eV, thereby constraining them to have really small masses compared to any other massive particle [25].

1.1.2 Detecting the neutrinos

The first direct observation of neutrinos was in 1956 by Reines and Cowan [26]. They directed a flux of $\bar{\nu}_e$ from a beta decay into a water target and detected it using inverse beta decay. The produced positron annihilates with an electron in the medium to give two characteristic 0.51 MeV photons. At the same time the

produced neutron is absorbed by $CdCl_2$ in the medium and emits photons a few μs later. These signals in coincidence were seen in their experiment and Reines won the Nobel prize in 1995 for the feat of detecting the first neutrinos.

The ν_μ was detected in 1962 at the Brookhaven National Laboratory through the decays of pions to muons and its associated neutrino [27]. The direct observation of the third generation ν_τ, took place in 2000 at the DONUT experiment at CERN [28].

One can determine the number of neutrino species with mass less than half the mass of Z through the invisible decay width of Z. The LEP experiment gives a very accurate measurement of $N_\nu = 2.994 \pm 0.012$ [29]. Cosmological data that constraint the number of neutrino flavours suggest an upper limit on N_ν to be 3 [25]. However, each of these measurements come with several caveats and it is not discounted that there could exist more neutrino flavours.

1.1.3 Parity and weak interaction

In 1957 Lee and Yang proposed that parity is violated in the weak interactions [30]. This solved the so called $\tau - \theta$ puzzle. Experiments by Wu et al [31] and Telegdi et al [32] among others, soon verified this. Both the above experiments which violated parity maximally since only left-handed neutrinos participate in weak interactions. This subsequently led to the $V - A$ model [33, 34] of weak interactions, which modified the 4-Fermi interaction involving beta decay to be of the form

$$\frac{G_F}{\sqrt{2}}[\bar{p}\gamma_\mu(c_V - \gamma_5 c_A)n][\bar{e}\gamma^\mu(1-\gamma_5)\nu] \quad ,$$

to incorporate parity violation. In SM, neutrinos interact only via weak interactions: they interact with W boson through the charged current interaction that gives rise to the term

$$\mathcal{L}_{CC} = [g/(2\sqrt{2})]\bar{\ell}\gamma^\mu(1-\gamma_5)\nu W^-_\mu + h.c. \tag{1.1}$$

in the SM Lagrangian. The interaction with Z boson is the neutral current interaction that gives rise to the term

$$\mathcal{L}_{NC} = [g/(2\cos\theta_W)]\bar{\nu}\gamma_\mu(1-\gamma_5)\nu Z^\mu \tag{1.2}$$

in the SM Lagrangian. The left-chiral projection operator $P_L \equiv (1-\gamma_5)/2$ ensures that only left-handed neutrinos $\nu_L \equiv [(1-\gamma_5)/2]\nu$ and right-handed antineutrinos $\bar{\nu}_R \equiv \bar{\nu}(1+\gamma_5)/2$ take part in the interactions which naturally gives rise to parity violation.

As we saw, neutrinos played a crucial role in the understanding of the weak interaction and SM. They also helped unravel the nuclear sub-structure by way of deep inelastic scattering (DIS) experiments. More recently, the first clear signal of physics beyond SM were revealed by the solar and atmospheric neutrinos. We discuss the solar and atmospheric neutrino problems to motivate the paradigm of massive neutrinos and neutrino oscillations as a solution of these problems.

1.1.4 Solar neutrinos

The sun radiates energy that is produced in nuclear fusion reactions that take place inside its core. The major reaction is $4p \rightarrow^4 He + 2e^+ + 2\nu_e$, though there are other reactions that produce heavier elements like Be, B and emit ν_e. The ν_e is the only neutrino species that can be produced in these nuclear reactions and their energies are about $(0.1 - 15)$ MeV.

Figure 1.1 shows the energy spectra of neutrinos produced in various reactions inside the sun, according to what is called the standard solar model (SSM). The electroweak theory predicts the shapes of the spectra, and the absolute magnitudes of the fluxes are calculated from SSM to be about $6 \times 10^6\ cm^{-2}s^{-1}$ [35].

The first indication that something was missing, came from the observation of solar neutrinos by the chlorine experiment of Davis et al [36]. The data from the gallium experiments i.e. GALLEX [37] and SAGE [38] also suggested that the flux of ν_e from the sun was smaller than expected by almost a factor of two. The Kamiokande (and later Super-Kamiokande) water Cherenkov experiment also detected a lower than expected ν_e flux [39]. The fluxes observed in these experiments were not the same, and it only added to the mystery. This could happen because these experiments detected ν_e in different energy ranges. It was thus apparent that whatever the mechanism of flux depletion, needed to be energy dependent. Neutrino decay and/or magnetic moment were considered as possible solutions to the problem but they do not solve the problem. Neutrino

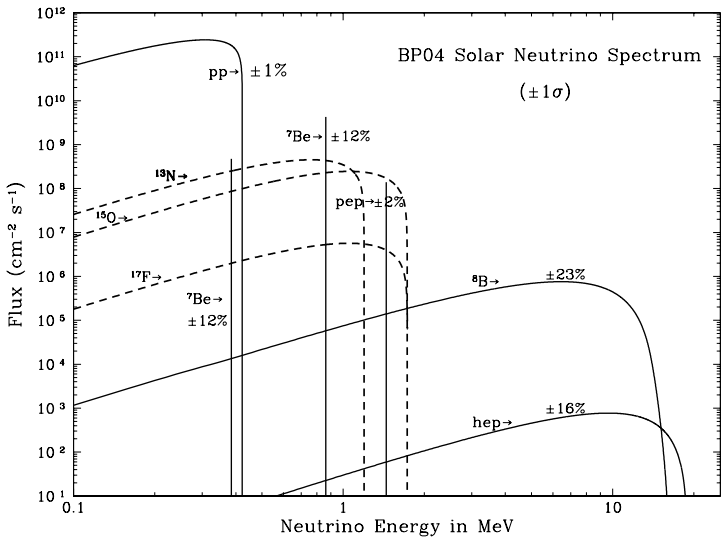

Figure 1.1: The solar neutrino fluxes predicted in the SSM. Figure taken from reference [35].

oscillations and matter effects seemed to be the dominant reason for the deficit. With the data from the SNO [40], this hypothesis has been confirmed, and it also finds that the SSM prediction for the total flux, a quantity that is not affected by oscillations, to be completely consistent with what is measured. That also strengthens our belief in SSM.

1.1.5 Atmospheric neutrinos

The Earth receives cosmic rays, comprising mainly protons, from all over the universe. The cosmic rays, upon interaction with the nuclei in the atmosphere, produce pions and kaons. Both pions and kaons decay predominantly into muons and muon neutrinos:

$$\pi^+ \to \mu^+\nu_\mu,\ \pi^- \to \mu^-\bar{\nu}_\mu,\ K^+ \to \mu^+\nu_\mu,\ K^- \to \mu^-\bar{\nu}_\mu \quad .$$

The muons then decay into electrons, one neutrino and one antineutrino:

$$\mu^- \to e^-\bar{\nu}_e\nu_\mu,\ \mu^+ \to e^+\nu_e\bar{\nu}_\mu \quad .$$

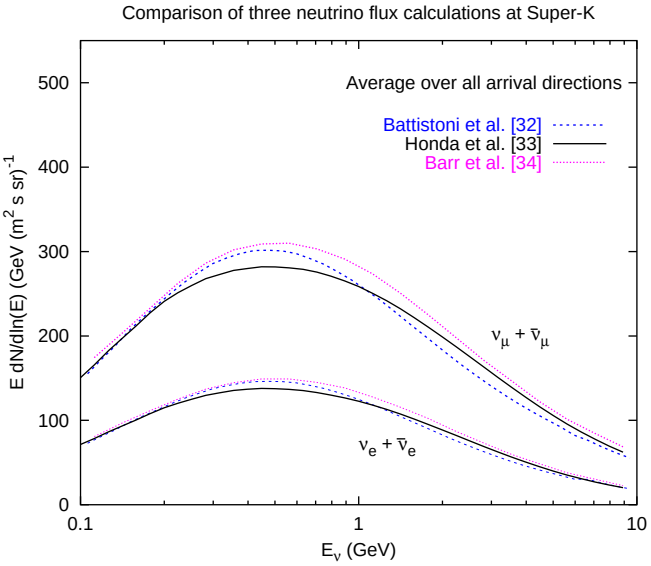

Figure 1.2: The atmospheric neutrino flux predicted in various models. Figure taken from reference [41].

As long as the detector does not distinguish between neutrinos and antineutrinos, this effectively means that the cosmic rays produce muon and electron neutrinos in the ratio 2:1. The energies of these neutrinos are about $(0.1 - 10)$ GeV. The fluxes of various neutrinos is predicted using a Monte Carlo simulation of the atmosphere as a detector with which the cosmic ray protons interact. Various groups calculate the expected atmospheric neutrino flux and calculated flux has a small dependence on the angular direction because of the presence of magnetic fields. Figure 1.2 shows the expected flux averaged over all angles, as calculated by various groups.

The first hint that something was missing in our understanding of atmospheric neutrinos came from the observation at the Kamiokande detector [42], that the muon-electron ratio was much smaller than 2. The model dependence of the predictions of atmospheric neutrino fluxes can be held "guilty" in this case, but what could not be dismissed so easily was that the ν_e flux remained unaffected. The most puzzling aspect was the zenith angle dependence of the fluxes. One expects that at higher energies (multi-GeV) we receive a higher flux from the

region near horizon (as compared to the zenith) because the mesons have longer flight-time to decay. The low energy neutrinos (sub-GeV) are unaffected because they are produced from low energy mesons which have a short lifetime anyway. One also expects a small dependence on zenith angle due to earth's magnetic field. What is seen, is that the ν_e flux is almost exactly what one expects, but the low energy ν_μ flux is depleted, more so for upcoming events. At high energies though, the ν_μ flux is depleted only for upcoming events and the downcoming flux is close to expectation. Remarkably, all these details are explained by neutrino oscillations.

1.1.6 Reactor and accelerator neutrinos

Nuclear reactors produce a large number of ν_e from their fission reactions. The energy of these neutrinos are of the order of 1 MeV. Accelerators produce neutrinos of energies about $(1 - 10)$ MeV. While much of the initial excitement about neutrinos came from the solar and atmospheric neutrinos, reactor and accelerator neutrino beams are a much better calibrated source and have been used very efficiently to nail down the oscillation scenario. In particular the data from KamLand [43], which detects neutrinos from several nearby reactors, helped confirm the oscillation scenario. Geo-thermal neutrinos, which provide a background at low energies, are also typically detected at detectors sensitive to reactor neutrino energies.

1.1.7 Supernova neutrinos

A supernova (SN) explosion is one of the strongest neutrino sources. The gravitational binding energy of the SN, of the order of 10^{53} ergs, is released almost completely ($\sim 99\%$) in the form of neutrinos and antineutrinos of all flavours and energies between $(5 - 80)$ MeV. These neutrinos propagate through the matter of the exploding star and thus details of the space and time dependent density profile of the star are encoded in the emitted flux of neutrinos. This may allow one to study the matter distribution inside the SN [20, 21] by studying the pattern of flavour conversion of the neutrinos that are detected from the explosion. Bounds on magnetic moments and decay rates are also typically very strong in

the case of SN neutrinos. The observation of 19 neutrinos from the SN 1987A [44, 45] itself constrains quite strongly the decay rates, magnetic moments and other properties. A high statistics signal from a galactic SN promises to provide a wealth of information. There is also a diffuse supernova neutrino background (DSNB) due the neutrinos coming to us every moment, from all the past SN explosions in the Universe which may also be possible to observe [46]. There are other cosmological sources of neutrinos, in particular relic neutrinos, however we shall not digress into a discussion of those.

1.2 Our present understanding

Taking into account all the existing data, except results from LSND [47] which remain to be confirmed/ruled out by Miniboone, we now have a global picture. It involves a deviation from SM by postulating neutrinos to have mass. We have three active neutrino flavours ν_e, ν_μ, ν_τ that are the eigenstates of the weak interaction. They are related to the three neutrino mass eigenstates ν_1, ν_2, ν_3 (with masses m_1, m_2, m_3 respectively) by the PMNS mixing matrix $U \equiv U_{PMNS}$, which is parametrised using three angles θ_{12}, θ_{23}, θ_{13} and a phase δ. The phase is important for CP violation in the lepton sector. A global analysis of neutrino data [48] tells us the magnitudes of neutrino mass square differences Δm^2_{21} and Δm^2_{31}, and the angles θ_{12} and θ_{23}.

There is presently only an upper limit on θ_{13}. The sign of Δm^2_{31}, which tells us whether the mass ordering (also referred as hierarchy) is normal or inverted, is not known. We don't know the absolute scale of neutrino mass either, which will tell us whether the masses are quasi-degenerate or hierarchical. There is no measurement of δ yet, and measurement of CP violation in lepton sector will be a big challenge. Also unknown is whether the mass term for neutrinos is of Dirac or Majorana nature. In case the neutrinos are Majorana fermions, there will be two more phases that can appear in the mixing matrix, whose physical significance is not well understood. There are numerous experiments dedicated to address one or more of these unresolved issues [49]. All these questions are of importance in understanding the kind of physics we should expect beyond SM, and thus a detailed study to measure these quantities is essential. When there

are matter effects involved, there is an interplay of many of these parameters. Understanding matter effects is thus crucial for determination of many of these quantities.

1.3 Plan and scope of the thesis

We have advertised that neutrinos have played an important role in understanding the SM. We also claim that neutrino oscillation solves the solar and atmospheric neutrino problems. This is our first departure from the SM and confirms the importance of neutrinos as a valuable probe of weak physics beyond SM. We now need to justify the claim by showing how the neutrino deficit problems are solved. So, in chapter 2, we will treat neutrino oscillations in detail and show how the atmospheric neutrino problem gets explained. We will then focus our attention to the effect that ambient matter has on neutrinos propagating through it. We will see that it is essential to include matter effects to explain the solar neutrino problem. Then we will investigate the cases where there are sudden density fluctuations. We will see that there are novel phenomena that can take place in such situations. The experimental data relevant to such a case is limited and therefore it is an interesting playground for predictions. We introduce a mechanism that could enhance neutrino oscillations (which we call phase effect) and complete our formal analysis of neutrino oscillation. We conclude the chapter by discussing what can be inferred from an observation of the said phase effects. In chapter 3, we will use the above formalism in the context of SN neutrinos to understand the effect of sudden density changes in the medium. We will see that observation of SN neutrinos can in principle tell us a lot about the neutrino masses and mixing, as well as about the SN explosion dynamics. We will also investigate the practical possibility to detect the phase effects at present and planned detectors. Finally, we will state our conclusions and provide an outlook towards future directions of the work outlined in this thesis.

Chapter 2

Neutrino flavour conversions in matter

We will begin this chapter by reviewing some methods to calculate the extent of flavour conversion due to neutrino oscillations in vacuum and in matter. We shall focus our attention to neutrino conversions in matter, in particular, when the density of the medium changes quite abruptly in a small region giving rise to enhanced conversion. There exist different methods to approximately calculate the conversion probabilities and we will outline some of those. We then present our suggested method for calculating the conversion probabilities, which works reasonably well even if the density is not strictly decreasing or increasing along the trajectory of the neutrino. It also has an added advantage of reproducing the neutrino wavefuctions at the end of the trajectory, and not just the conversion probabilities. We conclude the chapter by discussing a new kind of enhancement in neutrino conversion.

2.1 Neutrinos in vacuum

2.1.1 Vacuum oscillations

The Dirac equation governs the time evolution of neutrinos. For ultra-relativistic neutrinos, chirality conservation holds good [17] and it is convenient to remove the spin structure from the equations of motion. We therefore operate by the

Dirac operator once more to arrive at the Klein Gordon equation,

$$\left(\frac{d^2}{dx^2} + m^2\right)|\nu\rangle = \frac{d^2}{dt^2}|\nu\rangle \quad . \tag{2.1}$$

Here, the state $|\nu\rangle$ is an n dimensional vector and m^2 is a n×n matrix for n flavours. We consider neutrinos with the same momentum [50], and the d^2/dx^2 term is proportional to unity (independent of flavour) and can be dropped because we are only interested in the relative phases between the eigenstates. Moreover, once the direction of propagation of the neutrino is specified, the above second order equation reduces to a first order equation that is the Schrödinger equation with an effective Hamiltonian. The effective Hamiltonian for a neutrino mass eigenstate with mass m_i is

$$H_i = \sqrt{p^2 + m_i^2} \approx p + \frac{m_i^2}{2p} \approx p + \frac{m_i^2}{2E} \quad , \tag{2.2}$$

when only terms linear in (m_i/E) are kept. Again ignoring the terms that are independent of flavour, we shall take the effective neutrino Hamiltonian to be

$$H_i = \frac{m_i^2}{2E} \quad . \tag{2.3}$$

Let us work in a two neutrino framework for clarity, and take ν_α and ν_β as the two neutrino flavour eigenstates. They will not be the same as the mass eigenstates [6] in general now that the neutrinos are taken to be massive. Let the mass eigenstates be ν_i and ν_j with masses m_i and m_j respectively. The flavour eigenstates are a linear combination of mass eigenstates:

$$\begin{aligned} \nu_\alpha &= \cos\theta\ \nu_i + \sin\theta\ \nu_j \\ \nu_\beta &= -\sin\theta\ \nu_i + \cos\theta\ \nu_j \quad . \end{aligned} \tag{2.4}$$

Writing the above equation in matrix notation we have,

$$\nu_a = U_{ai}\nu_i \ , \tag{2.5}$$

where a runs over (α, β) and sum over i is implied. For two-neutrino mixing, the mixing matrix U can be parametrised in terms of a single angle θ:

$$U = \begin{pmatrix} \cos\theta & \sin\theta \\ -\sin\theta & \cos\theta \end{pmatrix} \ . \tag{2.6}$$

If neutrinos are produced as a flavour eigenstate ν_α their time evolution will be given by

$$\begin{aligned} \nu_\alpha(t) &= \cos\theta\ \nu_i(t) + \sin\ \theta\ \nu_j(t) \\ &= \cos\theta\ e^{-\frac{im_i^2 t}{2E}}\nu_i(0) + \sin\theta\ e^{-\frac{im_j^2 t}{2E}}\nu_j(0) \quad . \end{aligned} \tag{2.7}$$

The probability that we observe the same flavour eigenstate ν_α at time t (called survival probability) is then

$$P_{\alpha\alpha} \equiv P(\nu_\alpha \to \nu_\alpha) = |{\nu_\alpha}^*\nu_\alpha(t)|^2 = 1 - \sin^2 2\theta \sin^2\left(\frac{\Delta m_{ji}^2 L}{4E}\right) \quad . \tag{2.8}$$

Here $\Delta m_{ji}^2 \equiv m_j^2 - m_i^2$, and we have replaced t by L, the distance travelled, since neutrinos travel with the speed of light. We will continue to replace t by x from now on. This probability is oscillatory in distance, and hence the nomenclature neutrino oscillation in vacuum. The observability of these oscillations depends on an interplay of three quantities Δm_{ji}^2, L and E. Given a Δm_{ji}^2 and a certain E, the distance scale over which one can observe the fluxes to oscillate are $L_{osc} \sim E/\Delta m_{ji}^2$. As the neutrino travels over distances much larger than L_{osc}, they oscillate many times over and we may not observe oscillations if the neutrinos decohere. At distances much shorter than L_{osc} the oscillations are anyway not observed because the neutrinos have not oscillated enough by then.

2.1.2 Looking at atmospheric neutrinos

We will now use the above formalism to explain the atmospheric neutrino problem. Let us analyse the atmospheric neutrino data shown in figure 2.1 from Super-Kamiokande (SK), which is a water Cherenkov detector.

The experimental data is in black, the expected flux without (after) accounting for oscillations is in red (green). We see that the data for electron-like neutrino events matches with the expected number of events. The muon-like sub-GeV events are always less than expected, the depletion being greater for negative $\cos\Theta$, i.e. upcoming events. The muon-like multi-GeV events match with the expected rate for $\cos\Theta > 0$, i.e. downgoing events (which travel $\sim$ 10km),

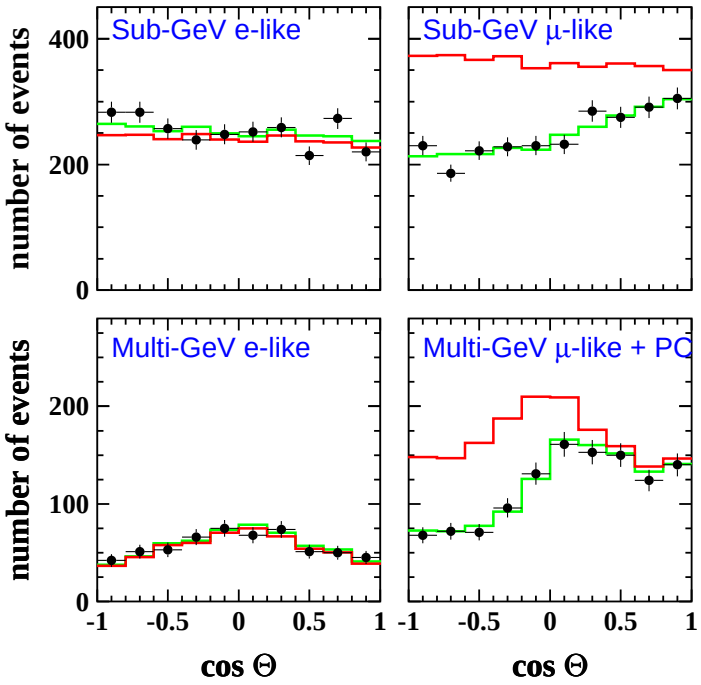

Figure 2.1: The zenith angle dependence of atmospheric neutrinos at SK. Figure taken from reference [42].

whereas a significant depletion is observed for the upcoming neutrinos (which travel $\sim$ 10000km).

All these features can be explained with the ansatz that the ν_μ oscillate away to ν_τ and that the ν_e remain almost unaffected while they travel from the point they are produced in the atmosphere, to the point they interact in the detector. Let us recall that the low energy neutrinos (sub-GeV) have smaller oscillation length that the high energy neutrinos (multi-GeV). The sub-GeV ν_μ can thus oscillate sufficiently even in the atmospheric column. This explains that for sub-GeV ν_μ events the depletion is not very strongly dependent on the zenith angle. This is not true for multi-GeV ν_μ which don't oscillate unless they travel a longer distance, explaining the markedly higher depletion for upcoming events. One can fit all the data to with two parameters Δm^2_{atm} and θ_{atm} which to parametrise $P(\nu_\mu \to \nu_\mu)$ using the equation (2.8). A full three neutrino analysis relates the effective Δm^2_{atm} to Δm^2_{21} and Δm^2_{31}. To a good approximation we find $\Delta m^2_{atm} \equiv$

Δm^2_{31} and $\theta_{atm} \equiv \theta_{23}$ [12]. Neutrino decay also could explain this experiment, but a characteristic dependence of the survival probability on L/E confirms [51] the oscillation hypothesis. The K2K experiment sends a ν_μ beam 250 km away to their detector and confirms the oscillation hypothesis independent of flux models [52]. There are more experiments lined up to confirm this solution and improve the precision of measurements. The best fit values for the mixing parameters are [42]

$$\Delta m^2_{atm} = (1.5 - 3.4) \times 10^{-3}\text{eV}^2 \quad , \quad \sin^2 2\theta_{atm} = 0.92 - 1.0 \quad (90\% c.l.) \tag{2.9}$$

2.2 Neutrinos in uniform matter density

In almost all physical situations, neutrinos travel through matter and interact weakly with it. When neutrinos travel through a medium, the amplitude for elastic forward scattering interactions with the electrons and nuclei therein adds up constructively with the amplitude of free propagation. This makes it necessary to including a potential energy term in the effective Hamiltonian. A potential due to charged current interactions is present only for electron neutrinos whereas the potential due to neutral current interaction is present for all flavours [8]. This is simply because the medium has very few muons or tauons, as opposed to electrons. The charge current and the neutral current potentials respectively are

$$V_{CC} = \sqrt{2} G_F N_e \tag{2.10}$$

$$V_{NC} = -G_F N_n / \sqrt{2} \tag{2.11}$$

where N_e is the number density of electrons and N_n is the density of neutrons in the medium. These expressions can be arrived at either using an analogy with optics as was done originally [8] or derived from a field theoretic treatment of the neutrino propagator as done in the references [53, 54, 55, 56]. The potential due to neutral current interaction V_{NC} is a matrix proportional to unity in the flavour basis and can be dropped. The charge current potential V_{CC}, which exists only for electron neutrinos, is not proportional to unity and must be kept. Thus the effect of the medium is to make the mass matrix non-diagonal even if it was almost

diagonal in vacuum. This is very different from ordinary vacuum oscillations because it arises due to an interaction and not merely by mixing of states.

Let us consider the mixing of ν_e with another flavour eigenstate ν_α, and write the effective Hamiltonian in the $(\nu_e\ \nu_\alpha)$ basis as

$$H_f = U \begin{pmatrix} m_1^2/(2E) & 0 \\ 0 & m_2^2/(2E) \end{pmatrix} U^\dagger + \begin{pmatrix} V_{NC} & 0 \\ 0 & V_{NC} \end{pmatrix} + \begin{pmatrix} V_{CC} & 0 \\ 0 & 0 \end{pmatrix} \quad (2.12)$$

Since we can drop an overall global phase the above Hamiltonian is equivalent to

$$H_f = \frac{1}{4E} \begin{pmatrix} -\Delta m^2 \cos 2\theta + 2A & \Delta m^2 \sin 2\theta \\ \Delta m^2 \sin 2\theta & \Delta m^2 \cos 2\theta \end{pmatrix} \quad (2.13)$$

as far as the mixing angle and the difference between the eigenvalues is concerned. Here $\Delta m^2 \equiv m_2^2 - m_1^2$ and $A \equiv 2E\ V_{CC}$. In matter, the eigenvalues of the matrix in equation (2.13) are

$$\frac{m_{1m/2m}^2}{2E} = \frac{1}{2E}\left(\frac{A}{2} \mp \frac{1}{2}\sqrt{(\Delta m^2 \cos 2\theta - A)^2 + (\Delta m^2 \sin 2\theta)^2}\right) \quad . \quad (2.14)$$

Thus, the effective Δm^2 in matter becomes

$$\Delta m_m^2 \equiv m_{2m}^2 - m_{1m}^2 = \sqrt{(\Delta m^2 \cos 2\theta - A)^2 + (\Delta m^2 \sin 2\theta)^2} \quad . \quad (2.15)$$

The effective Hamiltonian H_f can be diagonalised by a rotation matrix U as given in equation (2.6), with the mixing angle θ_m in matter

$$\tan 2\theta_m = \frac{\Delta m^2 \sin 2\theta}{\Delta m^2 \cos 2\theta - A} \quad . \quad (2.16)$$

The thing to note is that even if the mixing angle θ in vacuum were small, the matter effects can give rise to large effective mixing angle θ_m. This is called the Mikheyev-Smirnov-Wolfenstein (MSW) resonance [9, 10], and occurs when

$$A = \Delta m^2 \cos 2\theta \quad . \quad (2.17)$$

In a medium of constant electron density, the effective values of Δm^2 and the mixing angle change, but the remaining dynamics stays the same as in the vacuum case. As an example, the flavour conversion probability is

$$P_{e\mu} = \sin^2 2\theta_m \sin^2\left(\frac{\Delta m_m^2 L}{2E}\right) \quad . \quad (2.18)$$

Let us remark at this stage, that the solution to the atmospheric neutrino problem cannot be ν_μ oscillating away to a sterile neutrino ν_s, which has no SM interactions, because then we would have seen the matter effects on ν_μ relative to ν_s. The matter effects for ν_μ and ν_τ are same, keeping our earlier vacuum analysis valid.

2.3 Neutrinos in monotonically changing material density

Neutrinos travel through varying matter densities in many physical situations (e.g. through the earth or supernovae) where the extent of flavour conversion depends not only on the matter density but also the gradient of the density. To analyse neutrino conversions in such a situation is in general complicated. For some special forms of the density variations we can exactly solve the propagation equations, see reference [57] and the references therein. Specifically, the case of exponentially decreasing density is exactly solvable, and approximates the density variation inside the sun quite well. In most other cases, one has to settle for an approximate solution. If a small parameter exists in the problem, then the expressions for the amplitude of neutrinos conversion can be arranged in a perturbative expansion in that parameter. We illustrate this idea using a perturbation theory in the mixing angle, which is taken to be small. In the most general case, one has to compute the neutrino wavefunctions through arbitrary density variations by numerically solving the differential equation that governs their propagation.

2.3.1 LSZ approximation

For most realistic density profiles we cannot solve the problem exactly. We will see in this section that if the density changes very gradually, then we can think of the mass eigenstates as propagating independent of each other. This allows a calculation of the conversion probability of one mass eigenstate to another, assuming the density variation to be almost linear around the MSW resonance.

Let $U(\theta_m)$ be the unitary matrix that diagonalises the effective Hamiltonian locally in matter. Note that θ_m is a function of position. Then we have

$$\begin{pmatrix} \nu_{1m} \\ \nu_{2m} \end{pmatrix} = U^\dagger(\theta_m) \begin{pmatrix} \nu_e \\ \nu_\mu \end{pmatrix} \quad . \tag{2.19}$$

The Schrödinger's equation then gives the evolution of the neutrino states as

$$\begin{aligned} i\frac{d}{dx}\begin{pmatrix} \nu_{1m} \\ \nu_{2m} \end{pmatrix} &= i\frac{dU^\dagger(\theta_m)}{dx}\begin{pmatrix} \nu_e \\ \nu_\mu \end{pmatrix} + iU^\dagger(\theta_m)\frac{d}{dx}\begin{pmatrix} \nu_e \\ \nu_\mu \end{pmatrix} \\ &= \begin{pmatrix} m_{1m}^2/(2E) & -id\theta_m/dx \\ id\theta_m/dx & m_{2m}^2/(2E) \end{pmatrix}\begin{pmatrix} \nu_{1m} \\ \nu_{2m} \end{pmatrix} \quad . \end{aligned} \tag{2.20}$$

For the case of a very slowly changing density, the off-diagonal elements in equation (2.20) are always much smaller than $|m_{2m}^2 - m_{1m}^2|/(2E)$, so that the mass eigenstates in matter, ν_{1m} and ν_{2m}, propagate almost independently of each other, without mixing. This limit corresponds to

$$\frac{\Delta m^2}{(\Delta m_m^2)^2}\sin 2\theta \frac{dA}{dx} \ll \frac{\Delta m_m^2}{2E} \tag{2.21}$$

when we substitute for θ_m in matter. The condition for "adiabaticity", i.e. for the mass eigenstates in matter not to mix, the reduces to

$$\gamma \equiv \frac{\Delta m^2}{2E}\frac{\sin^2 2\theta}{\cos 2\theta}\left(\frac{1}{A}\frac{dA}{dx}\right)^{-1}_{res} \gg 1 \quad . \tag{2.22}$$

If the above inequality is violated only in a small region of space, one can still consider the mass eigenstates to travel independently of each other in the remaining region. The inequality is broken maximally near the MSW resonance, where the mass eigenvalues are closest to being degenerate. Some fraction of each mass eigenstate gets converted to the other at the point where the adiabaticity condition is violated. This fraction is the conversion probability. Note that this statement is made using the language of probabilities and not amplitudes. The probability of "jump" of one mass eigenstate in matter to another can be computed by using the Landau Stückelberg Zener (LSZ) approximation [58, 59]. The jump probability is approximately

$$P_{jump} = Exp(-\pi\gamma/2) \tag{2.23}$$

where γ is calculated at the MSW resonance. The assumption that goes into this result, is that the density varies linearly around the MSW resonance, and then the exact result for the case of linear variation of density is used. This result can be derived using contour integrals as in the reference [57]. There is an improved treatment [60] where it is argued that γ be calculated at the point of maximal violation of adiabaticity (PMVA) defined as the postion where the ratio of the diagonal term to off diagonal term of the matrix in equation (2.20) is minimum. The following equation defines x_{PMVA}:

$$\frac{d}{dx}\frac{\Delta m_m^2}{(d\theta_m/dx)} = 0 \quad . \tag{2.24}$$

The jump probability thus depends on Δm^2, mixing angle, the density profile encountered by the neutrinos, as well as the neutrino energy. This is again a phenomenon that is quite different from neutrino oscillations in either vacuum or matter of constant density. Here, the conversion happens because the mass eigenstates are not the same all over space and there is a finite tunneling probability for a mass eigenstate to transform to another at the point where the barrier is smallest, i.e close to the resonance or the PMVA. This probability of conversion of one mass eigenstate to another is identically zero if adiabaticity is not violated. We must also note the following: Adiabatic neutrino flavour conversion depends sinusoidally on the distance between source and detector. Non-adiabatic neutrino conversion on the other hand, due to a steep density gradient, is not dependent on the distance between source and detector.

2.3.2 Looking at solar neutrinos

Let us now address the solar neutrino problem, with the aid of the formalism developed in the last section. The experiments suggested that the detected flux of ν_e events was about a factor of two less than what was expected. The depletion seemed to be energy dependent only at the low energies, i.e. energies comparable to the thresholds of chlorine and gallium detectors. We need to explain the deficit and the energy independence of the depletion.

The answer to the problem is the so-called LMA-MSW scenario [61]. It corresponds to (for $E > 5$ MeV) a completely adiabatic transition ($P_{jump} = 0$) at the

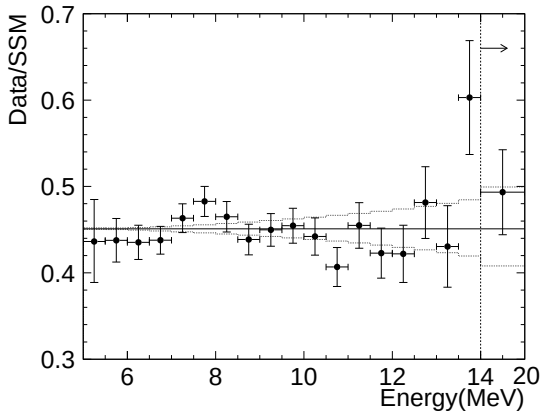

Figure 2.2: Observed survival probability of solar ν_e as a function of energy. Figure taken from the reference [39].

resonance the neutrinos undergo inside the sun. Thus, ν_e, which are produced as ν_{2m} inside the sun (because at high densities where $A \gg \Delta m^2_{\odot}/(2E)$, so that $\theta_m \approx \pi/2$ and $\nu_e \approx \nu_{2m}$), travel through the matter inside the sun and emerge from the sun as ν_2. These ν_2, being mass eigenstates in vacuum, reach the earth as ν_2, where they are detected as ν_e with a probability $\sin^2\theta_{\odot}$ and as $\nu_{\mu/\tau}$ with a probabilty $\cos^2\theta_{\odot}$.

The data from SK [39], as shown in figure 2.2, shows no energy dependence for $E > 5$ MeV. This strongly suggests that the oscillations are getting averaged out. We remember that the SuperKamiokande detects ν_e and $\nu_{\mu/\tau}$ via elastic scattering (ES) on electrons, but with a factor of 6 lower cross-section for the latter. This means that the experiment is sensitive to the quantity $sin^2\theta_{\odot} + (1/6)cos^2\theta_{\odot}$ which is approximately 0.46. That gives a simple estimate of $\theta_{\odot} \approx 35°$. At lower energies ($E < 5$) MeV there is no MSW resonance and the conversion rate is slightly different.

The clinching evidence in favour of the oscillation hypothesis came from the SNO (Sudbury Neutrino Observatory) experiment that used heavy water as the detector,and detected neutrinos through three reactions [40]. Elastic scattering ($\nu + e^- \rightarrow \nu + e^-$), as we saw, can be said to be sensitive to the combination of fluxes $\Phi_e + (1/6)\Phi_{\mu+\tau}$, which is constrained to be in the green band in figure 2.3.

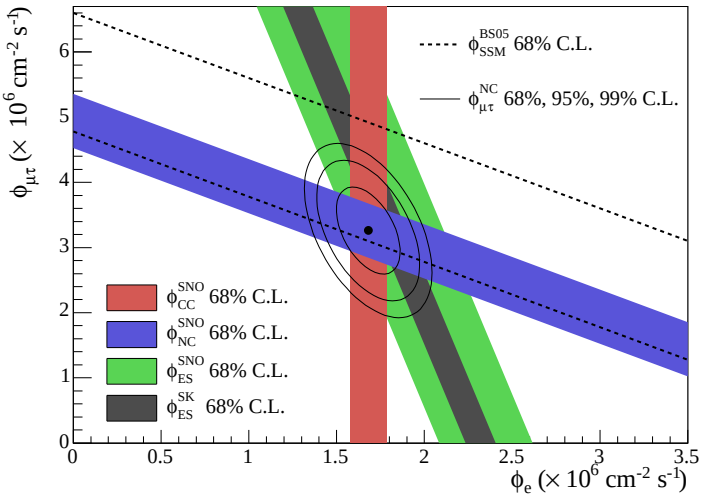

Figure 2.3: The results from SNO on various linear combinations of ν_e and $\nu_{\mu/\tau}$ fluxes. Figure taken from the reference [40].

Charged current (CC) ($\nu_e + d \rightarrow p + p + e^-$), which can take place only with ν_e, and hence sensitive to Φ_e, which is constrained to the red band. Neutral current (NC) ($\nu + d \rightarrow n + p + \nu$), which is blind to the flavour of the neutrino species and hence effectively measures $\Phi_e + \Phi_\mu + \Phi_\tau$, constrained in the blue band. It also agrees with the measurement of $\Phi_e + (1/6)\Phi_{\mu+\tau}$ by Super-Kamiokande shown as the black band.

As can be clearly seen, the SSM prediction is bang on the NC flux that is blind to oscillations. This confirms our belief on SSM as it predicts a correct total flux. What is also borne out, is that the depleted ν_e are oscillating to $\nu_{\mu/\tau}$. It also rules out a dominant role of sterile neutrinos in the solar neutrino oscillations. The KamLand experiment confirmed the LMA solution and measured the values of $\Delta m^2_\odot$ and $\theta_\odot$ to a much better accuracy [43]. A three neutrino analysis relates the $\Delta m^2_\odot$ and $\theta_\odot$ to Δm^2_{21} and θ_{12} respectively, in the limit $\theta_{13} = 0$ and $\Delta m^2_\odot \ll \Delta m^2_{atm}$. The best fit values for the mixing parameters are [62]

$$\Delta m^2_\odot = (7.2 - 9.5) \times 10^{-5}\text{eV}^2 \quad , \quad \sin^2\theta_\odot = 0.21 - 0.37 \quad (3\sigma) \quad . \tag{2.25}$$

2.3.3 Perturbative expansion in a mixing angle

We saw that one can calculate neutrino survival probabilities in the LSZ approximation. However that method only gives survival and conversion probabilities and not the amplitudes of the neutrino wavefunctions after it crosses the variable density medium. It is sometimes desirable to know the wavefunctions, as we shall find in the next section. In this section we will review one particular way to calculate the wavefunctions. The following method is based on a perturbative solution to the equations of motion.

Lets look at the propagation of flavour eigenstates. In this basis the density variation enters in a simpler way and its easier to solve. Let ν_β be the relevant linear combination of ν_μ and ν_τ. We have,

$$i\frac{d}{dx}\begin{pmatrix}\nu_e\\ \nu_\beta\end{pmatrix} = \frac{1}{4E}\begin{pmatrix}A(x)-\Delta m^2\cos 2\theta & \Delta m^2\sin 2\theta\\ \Delta m^2\sin 2\theta & -A(x)+\Delta m^2\cos 2\theta\end{pmatrix}\begin{pmatrix}\nu_e\\ \nu_\beta\end{pmatrix} \quad (2.26)$$

where $A(x) \equiv 2EV(x) \equiv 2\sqrt{2}G_F Y_e \rho E/M_N$. We see that the potential depends on electron fraction Y_e, density of matter ρ, neutrino energy E and the average nucleon mass of the medium M_N. These two coupled first order equations give rise to the second order equation

$$-\frac{d^2}{dx^2}\nu_e - (\phi^2 + i\phi')\nu_e = \eta^2\nu_e \quad (2.27)$$

where

$$\phi(x) = \frac{1}{4E}[A(x) - \Delta m^2\cos 2\theta]\ , \quad \eta = \frac{\Delta m^2}{4E}\sin 2\theta \quad (2.28)$$

and prime ($'$) denotes derivative with respect to x. In order to find the survival probability of ν_e, we solve for the ν_e wavefunction with the initial conditions $\nu_e(0) = 1$, $\nu_\beta(0) = 0$. These conditions are equivalent to

$$\nu_e(0) = 1\ , \quad i\left.\frac{d\nu_e}{dx}\right|_0 = \phi(0)\ . \quad (2.29)$$

The reference [63] illustrates some simple perturbative methods to solve the above equations. We remark that the perturbation in $\hbar$ will not capture non-adiabatic

effects at first order in perturbation theory. The "logarithmic perturbation" approximation solves the differential equation (2.27) for small mixing angles by choosing

$$g \equiv 1 - \cos 2\theta \tag{2.30}$$

as the small expansion parameter. Denoting

$$\nu_e = e^{S(x)} , \quad \text{with} \quad S'(x) = c_0(x) + g c_1(x) + O(g^2) \tag{2.31}$$

so that

$$\nu_e(x) = \exp\left(\int_0^x dx_1 c_0(x_1) + g \int_0^x dx_1 c_1(x_1) + O(g^2) \right) , \tag{2.32}$$

the solution becomes

$$\begin{aligned} \nu_e(x) \;\; = \;\; & \exp\left(-\frac{iQ(x)}{2} - g\frac{i\Delta m^2 x}{4E} \right. \\ & \left. - g\frac{(\Delta m^2)^2}{2\ (2E)^2} \int_0^x dx_1 e^{iQ(x_1)} \int_0^{x_1} dx_2 e^{-iQ(x_2)} \right) + \mathcal{O}(g^2) \end{aligned} \tag{2.33}$$

Here we have defined the "accumulated phase"

$$Q(x) \equiv \frac{1}{2E} \int_0^x dx_1 \left[A(x_1) - \Delta m^2 \right] . \tag{2.34}$$

The survival probability $P_{ee}(x) \equiv P(\nu_e \to \nu_e)$ at $x = X$ then becomes

$$P_{ee}(X) = \exp\left(-g\frac{(\Delta m^2)^2}{2\ (2E)^2} \left| \int_0^X dx_1 e^{iQ(x_1)} \right|^2 \right) + O(g^2) . \tag{2.35}$$

The integral in the above expression can be evaluated using the stationary phase approximation. The integral oscillates rapidly unless $Q'(x) \approx 0$. So the entire contribution to the integral can be taken to be from the saddle point x_s, which is the point where $Q'(x_s) = 0$, i.e.

$$A(x_s) = \Delta m^2 . \tag{2.36}$$

Note that this is also the resonance point in the small angle limit.

For a monotonic density profile, there is only one saddle point x_s and the survival probability is

$$P_{ee} \approx \exp\left(-g\frac{\pi(\Delta m^2)^2}{2E|A'(x_s)|} \right) , \tag{2.37}$$

which agrees with the LSZ jump probability [58, 59] in the limit of small mixing angle, and hence small g, even when $P_{ee} \sim 1$.

2.4 Neutrinos through non monotonic density variation

The method illustrated in the previous section works for non-monotonic density profiles also, once we make a small extension. However, the effects that are observed are far from trivial. The most important difference between a monotonic density profile and a non-monotonic density profile is that, for a monotonic profile there is only one saddle point whereas for a non monotonic density there can be several of them. In that case one gets contributions from all the saddle points of the integrand in equation (2.35). If the saddle points are far apart and the integrals about each of them die out very fast, then the contributions from each of them should be added independently of each other but taking care of the relative phases between them.

2.4.1 Perturbative expansion in a mixing angle

For a non-monotonic density profile, neutrinos can experience more than one resonance at the same density but at different positions. In that case $Q'(x) = 0$ at more than one point. If the resonances are sufficiently far apart, the contributions from each of them may be added independently of each other. Their total contribution to the integral in equation (2.35) is

$$\int_0^X dx e^{iQ(x)} \approx \sum_i e^{i\alpha_i} e^{iQ(x_i)} \left(\frac{4\pi E}{|A'(x_i)|}\right)^{1/2} \tag{2.38}$$

where i runs over all the saddle points. Note that $\alpha = \pi/4$ if $A'(x_s) < 0$ and $\alpha = 3\pi/4$ if $A'(x_s) > 0$. The probability calculated using equation (2.35) now has terms which depend on the differences between the integrated phases

$$\Phi_{ij} \equiv Q(x_j) - Q(x_i) + \alpha_j - \alpha_i = \int_{x_i}^{x_j} \frac{1}{2E}\left[A(x) - \Delta m^2\right] dx \ . \tag{2.39}$$

In general,

$$P_{ee}(X) = \exp\left[-g\left(\sum_i a_i^2 + 2\sum_{i<j} a_i a_j \cos\Phi_{ij}\right)\right] + \mathcal{O}(g^2) \tag{2.40}$$

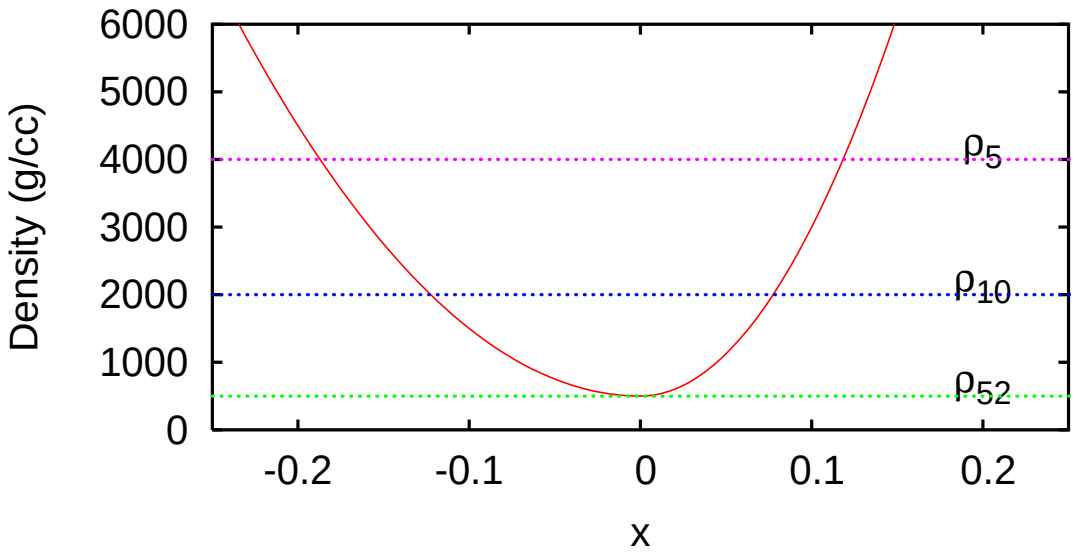

Figure 2.4: Toy density profile of equation (2.43).

where

$$a_i \equiv \left(\frac{\pi(\Delta m^2)^2}{2E|A'(x_i)|} \right)^{1/2} . \tag{2.41}$$

For example, when there are only two saddle points the survival probability is given by

$$P_{ee} = \exp(-g a_1^2) \exp(-g a_2^2) \exp(-2g a_1 a_2 \cos \Phi_{12}) . \tag{2.42}$$

The first two factors in equation (2.42) are the individual LSZ jump probabilities for the two level crossings. The last factor gives rise to oscillations in P_{ee} as a function of energy. The oscillation pattern has its maxima at $\Phi_{12} = (2n+1)\pi$ and minima at $\Phi_{12} = 2n\pi$ where n is an integer.

We illustrate the validity and limitations of the small angle approximation with a toy density profile, shown in figure 2.4.

$$\rho(x) = \begin{cases} a + b_1 x^2 & (x < 0) \\ a + b_2 x^2 & (x > 0) \end{cases} , \tag{2.43}$$

The parameter values are chosen to be, $a = 500$ g/cc, $b_1 = 10^5$ g/cc $/(10^8$ cm$)^2$ and $b_2 = 2.5 \times 10^5$ g/cc $/(10^8$ cm$)^2$. We also show the positions of resonance

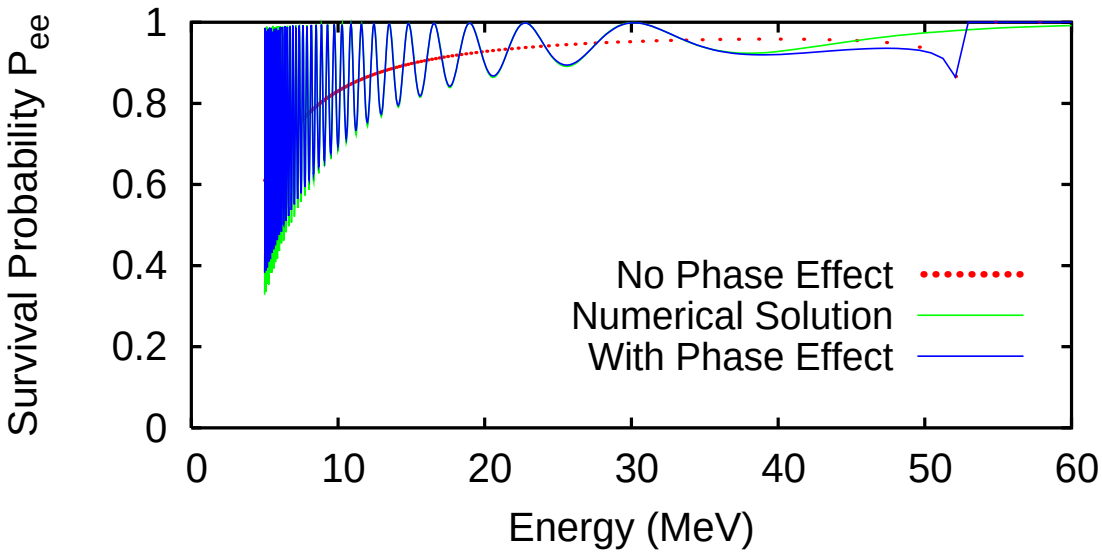

Figure 2.5: Survival probability P_{ee} as a function of energy for $\theta = 0.02$ rad $\approx 1.1°$.

densities for various energies, which are given by

$$\rho_E(g/cc) \approx \pm\Delta m^2(eV^2)\cos 2\theta/(2 \times 7.6 \times 10^{-8} Y_e E(MeV)). \tag{2.44}$$

The horizontal lines on the graph are the resonance densities for various energies (5, 10, 52 MeV) taking $\theta = 0.02$ rad $\approx 1.1°$, $Y_e = 0.5$ and $\Delta m^2 = 0.002\ eV^2$. Notice how the saddle points come closer for larger energies till $E = E_{R(max)} = 52$ MeV, after which there is no resonance.

Figure 2.5 shows the survival probability P_{ee} as a function of energy, both the exact numerical result and the result of our analytic approximation for small angles. Neutrinos are produced at $x \to -\infty$ and we calculate P_{ee} at $x \to \infty$ using our toy density profile. It can be seen that at such small angles ($\theta = 0.02$ rad $\approx 1.1°$), the approximation works extremely well. The green (light) curve is the numerically evaluated exact result. The blue (dark) curve is our solution with small angle approximation including the phase effects. The red (dotted) curve is the approximate solution if the phase effects are neglected or decoherence is assumed between successive resonances. Notice that our approximate solution

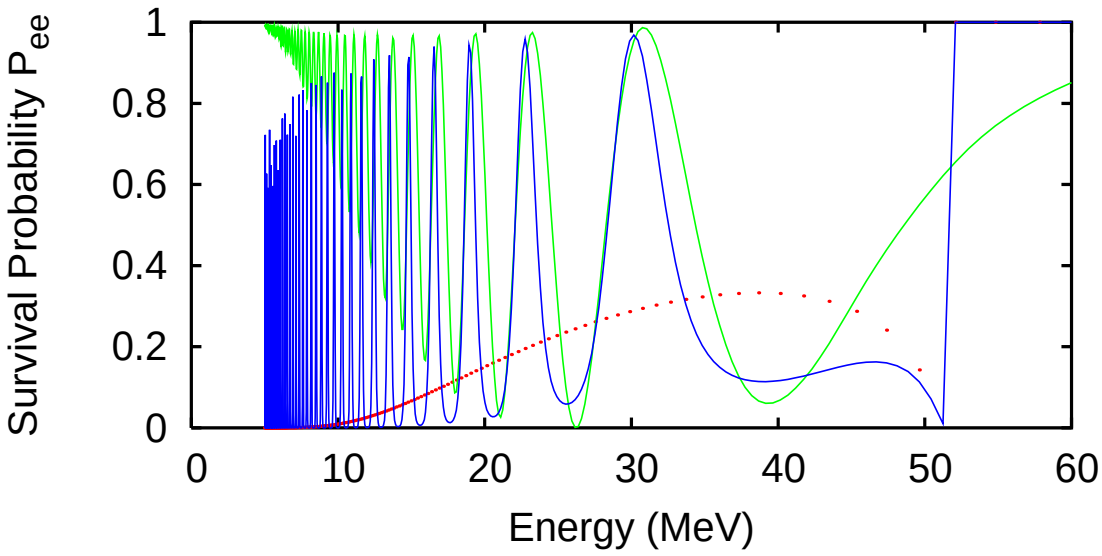

Figure 2.6: Survival probability P_{ee} as a function of energy for $\theta = 0.1$ rad $\approx 5.7°$. The convention for the lines is the same as that used in figure 2.5.

is valid only upto $E = E_{R(max)}$. Note that the amplitude of the oscillations is comparable to the deviation of the average survival probability from unity. That is, the oscillation effect is not a small effect. Indeed, the oscillation term is of the same order as the averaged effect, as can be seen from equation (2.42). Figure 2.5 also shows the average value of P_{ee} that one would have obtained if one naively combined the jump probabilities at the two resonances. Our analysis gives additional oscillations in the survival probability as a function of neutrino energy about this average value. This novel effect is what we call as the "phase effect," and is clearly significant as can be seen from the figure. An important feature of the oscillations is that the "wavelengths," i.e. the distances between the consecutive maxima or minima, are larger at larger E.

The resonances start overlapping at $E \approx E_{R(max)}$ (as defined in figure 2.4), which is where our approximation starts breaking down, as can be seen in figure 2.5. For $E > E_{R(max)}$, the neutrinos no longer encounter a strict resonance, and our approximation gives $P_{ee} = 0$ identically. However, the resonances have finite widths which may affect the conversion probabilities of neutrinos with

$E \approx E_{R(max)}$. The sharp jump observed in figure 2.5 at $E \approx 52$ MeV is therefore not a real effect, but a limitation of our technique.

The small angle approximation starts failing for larger angles and lower energies. Figure 2.6 shows that the amplitude at low energies is not calculated correctly for $\theta = 0.1$ rad $= 5.7°$. This is not surprising, if we notice that the expression for P_{ee} one gets from equation (2.42) assuming decoherence, matches with $P_1P_2 + (1-P_1)(1-P_2)$ only for small theta. However, note that the positions of maxima and minima of P_{ee} are still predicted to a good accuracy. We shall provide an argument (due to Dighe) in the next subsection that these can be computed accurately for the whole allowed range of θ_{13}, given the non-monotonic density profile between the two resonances.

2.4.2 Understanding the phase effects

Let us consider a toy density profile with only one minima (or maxima). A neutrino with energy E_k encounters two resonances R_1 and R_2 at $x = x_1$ and $x = x_2$ respectively, so that

$$\rho_{E_k} \equiv \rho(x_1) = \rho(x_2) \; . \tag{2.45}$$

let us assume Y_e to be a constant throughout the region of interest. Let us also assume that the propagation of neutrino mass eigenstates is adiabatic everywhere except in the resonance regions (x_{1-}, x_{1+}) and (x_{2-}, x_{2+}) around the resonance points x_1 and x_2 respectively. In the limit of small angles, the widths of the resonances are small:

$$\Delta\rho \approx \rho \tan 2\theta \; . \tag{2.46}$$

Therefore, $x_{1-} \approx x_1 \approx x_{1+}$ and $x_{2-} \approx x_2 \approx x_{2+}$. We shall work in this approximation, and shall use the notation $x_{i\pm}$ only for the sake of clarity wherever needed.

At $x \ll x_1$, the density $\rho(x) \gg \rho_{E_k}$, so that the heavier mass eigenstate ν_H is approximately equal to the flavour eigenstate ν_e. Let us start with ν_e as the initial state:

$$\nu_e(x \ll x_1) \approx \nu_H \; . \tag{2.47}$$

The mass eigenstate ν_H propagates adiabatically till it reaches the resonance region $x \approx x_1$:

$$\nu_e(x_{1-}) \approx \nu_H \ . \tag{2.48}$$

While passing through the resonance, unless the resonance is completely adiabatic, the state becomes a linear combination of ν_H and ν_L, the lighter mass eigenstate. Note that the phases of ν_H and ν_L can be defined to make their relative phase vanish at $x = x_{1+}$.

$$\nu_e(x_{1+}) = \cos\chi_1 \nu_H + \sin\chi_1 \nu_L \ , \tag{2.49}$$

where $P_1 \equiv \sin^2\chi_1$ is the "jump probability" at R_1 if it were an isolated resonance.

The two mass eigenstates ν_H and ν_L propagate to the other resonance R_2, gaining a relative phase in the process (the overall phase of the state is irrelevant):

$$\nu_e(x_{2-}) = \cos\chi_1 \nu_H + \sin\chi_1 \exp\left(i\int_{x_1}^{x_2} \frac{\Delta\tilde{m}^2}{2E}dx\right)\nu_L \ , \tag{2.50}$$

where $\Delta\tilde{m}^2$ is the mass squared difference between ν_H and ν_L in matter:

$$\Delta\tilde{m}^2(x,E) = \sqrt{[\Delta m^2\cos 2\theta - 2EV(x)]^2 + (\Delta m^2 \sin 2\theta)^2} \ . \tag{2.51}$$

The effect of the resonance R_2 may be parametrised in general as

$$\begin{pmatrix} \nu_H(x_{2+}) \\ \nu_L(x_{2+}) \end{pmatrix} = \begin{pmatrix} \cos\chi_2 & \sin\chi_2 e^{i\varphi} \\ -\sin\chi_2 e^{-i\varphi} & \cos\chi_2 \end{pmatrix} \begin{pmatrix} \nu_H(x_{2-}) \\ \nu_L(x_{2-}) \end{pmatrix} \ . \tag{2.52}$$

where $P_2 \equiv \sin^2\chi_2$ is the "jump probability" at R_2 if it were an isolated resonance.

From equation (2.33), one can deduce that in the limit $x_{2-} \approx x_{2+}$, we have $\varphi \approx Q(x_{2+} - x_{2-}) \approx 0$. The state $\nu_e(x_{2+})$ can then be written as

$$\begin{aligned} \nu_e(x_{2+}) \ &= \ \left[\cos\chi_2\cos\chi_1 + \sin\chi_2\sin\chi_1 \exp\left(i\int_{x_1}^{x_2}\frac{\Delta\tilde{m}^2}{2E}dx\right)\right]\nu_H \\ &+ \ \left[\cos\chi_2\sin\chi_1 \exp\left(i\int_{x_1}^{x_2}\frac{\Delta\tilde{m}^2}{2E}dx\right) - \sin\chi_2\cos\chi_1\right]\nu_L \ . \end{aligned} \tag{2.53}$$

For $x > x_{2+}$, the mass eigenstates travel independently and over sufficiently large distances, decohere from one another. At $x \gg x_2$, since $\rho(x) \gg \rho_{E_k}$, the

heavier mass eigenstate ν_H again coincides with ν_e and we get the ν_e survival probability as

$$P_{ee} = \left|\cos\chi_2\cos\chi_1 + \sin\chi_2\sin\chi_1\exp\left(i\int_{x_1}^{x_2}\frac{\Delta\tilde{m}^2}{2E}dx\right)\right|^2 \tag{2.54}$$

$$= \cos^2(\chi_1-\chi_2) - \sin 2\chi_1\sin 2\chi_2\sin^2\left(\int_{x_1}^{x_2}\frac{\Delta\tilde{m}^2}{4E}dx\right) . \tag{2.55}$$

If the phase information were lost, either due to decoherence or due to finite energy resolution of the detectors [64] the survival probability would have been

$$P_{ee_{(nophase)}} = P_1P_2 + (1-P_1)(1-P_2) \tag{2.56}$$

$$= \cos^2\chi_1\cos^2\chi_2 + \sin^2\chi_1\sin^2\chi_2 , \tag{2.57}$$

which matches with equation (2.55) when the $\sin^2(\int ..)$ term is averaged out to 1/2. This result is also recovered to first order in g from the equation (2.42).

The $\sin^2(\int ..)$ term in equation (2.55) gives rise to the oscillations in $P_{ee}(E)$. If two consecutive maxima of P_{ee} are at energies E_k and E_{k+1} such that $E_k > E_{k+1}$, then the condition

$$\int_{x_1(E_{k+1})}^{x_2(E_{k+1})}\frac{\Delta\tilde{m}^2(x,E_{k+1})}{2E_{k+1}}\,dx - \int_{x_1(E_k)}^{x_2(E_k)}\frac{\Delta\tilde{m}^2(x,E_k)}{2E_k}\,dx = 2\pi \tag{2.58}$$

is satisfied. The quantity $(E_k - E_{k+1})$ is the "wavelength" of the oscillations, as observed in the energy spectrum.

Note that $\Delta\tilde{m}^2(x,E)$ is equal to $|A(x)-\Delta m^2|$ in the small angle limit. Moreover, this quantity is rather insensitive to θ in the allowed range of θ_{13}. Therefore, it is not a surprise that the predictions of the positions of maxima and minima in the small angle approximation are accurate and robust in the whole range $\theta < 13^\circ$. However the perturbation theory in g fails at large mixing angles.

Since θ is small, the left hand side of (2.58) is approximately equal to the area of the region in the density profile plot enclosed by the densities ρ_{E_k} and $\rho_{E_{k+1}}$:

$$\mathcal{A} \approx 2\pi\frac{M_N}{\sqrt{2}G_FY_e} . \tag{2.59}$$

This simple fact allows us in principle, to partially reconstruct the density profile through the following procedure: Figure 2.7(a) shows a schematic plot of the

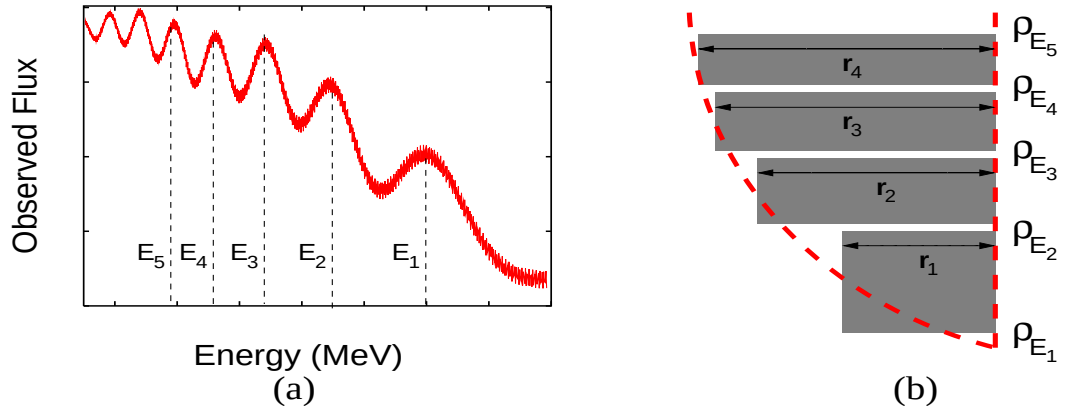

Figure 2.7: Reconstructing the density profile from the oscillations in the observed flux shown in (a). The area of each rectangle in (b) is equal to $\mathcal{A}$.

observed flux as a function of energy. Let E_k be the energies corresponding to the local maxima in the observed spectrum, with increasing k corresponding to decreasing energies. If we assume that $\rho_{E_k} \approx \rho_{E_{k+1}}$, the distance between $R_1$and R_2 in the region $\rho_{E_k} < \rho < \rho_{E_{k+1}}$ is then given by

$$r_k \approx \mathcal{A}/(\rho_{E_{k+1}} - \rho_{E_k}) \, . \tag{2.60}$$

This procedure may be repeated to estimate the separation of resonances for all the maxima that can be identified. If one of the branches of the density profile is steep enough to be approximated well by a density discontinuity, this procedure can be used to reconstruct the density profile of the other branch. We consider this special case because,it is relevant to supernova density profiles. Figure 2.7(b) indicates this procedure graphically. The resolution of $r(\rho)$ may be increased by using the local minima in addition to the maxima, taking into account that the phase between a minimum and the next maximum is half the phase between two consecutive maxima or minima.

Non-monotonic density profiles are encountered by neutrinos escaping from a core collapse supernova during the shock-wave propagation. If the phase effects are observable at neutrino detectors, the above procedure may help us reconstruct the shock-wave partially. This procedure for reconstructing the density profile is

somewhat crude, and the information obtained is only on the density profile along the line of sight. We also need to assume that neutrinos coming from different parts of the neutrinosphere encounter nearly the same density profiles. However, it is the only way we know as of now that can tell us about the density profile deep inside the astrophysical objects like supernovae, directly from the data. Moreover, note that this procedure is not affected by the uncertainties in the primary fluxes, since the positions of the maxima and minima are independent of the primary fluxes. Since neutrinos are the only particles that can, even in principle, carry information from so deep inside the exploding star, it is important to explore the feasibility of the detection of these phase effects. That will be the subject of the next chapter.

Chapter 3

Phase effects in neutrino conversions in a supernova

Density variation inside an exploding supernova (SN) is not monotonic and is expected to be very drastic. In such a situation non-adiabatic effects become important. We will, in this chapter, study the non-adiabatic effects of matter on neutrinos coming from a SN. Those neutrinos would encode useful information about neutrino masses and mixing, as well as about the internal structure of the SN. So a probable high-statistics signal from such an explosion will need to be decoded to obtain useful information about neutrinos and stellar structure. In the first section, we mention a few preliminaries about SN and neutrino fluxes expected from a SN. Subsequently, we use some knowledge of the primary fluxes and SN density profiles to calculate the neutrino signal observable at a detector on earth. The role of matter effects is discussed using the methods discussed in the previous chapter. We present our results on the role of phase effects in the context of SN neutrinos and discuss some of the aspects that we have ignored in our analysis before we end this chapter.

3.1 Supernova neutrinos

Let us start by recalling some facts about SN explosions and the neutrino fluxes expected from them. These aspects are not completely understood and most of

what we know comes from numerical hydrodynamic simulations of the exploding star. The discussion that follows is based on the text by Raffelt [65].

3.1.1 Explosion mechanism

A large star with more that 10 times the mass of the sun ($M_\odot$) becomes a red or a blue super giant in the final states of its life. Such stars usually have an onion like structure, with each successive inner shell producing successively heavier elements via nuclear reactions. The core is mainly made of iron, because iron is stable and does not undergo fusion. When the mass of the iron core reaches the Chandrasekhar limit ($\approx 1.4\ M_\odot$), the electron degeneracy pressure is insufficient to counter-balance the inward gravitational force. When nuclear fuel for fusion runs out, then the core starts collapsing in the absence of radiation pressure. As the core collapses to a radius of about 10 Km, the density reaches a few times the nuclear density and the core stiffens. The gravitational binding energy is mainly converted to neutrinos and antineutrinos of all flavours, which are copiously pair-produced inside the core of the SN. Most of these neutrinos cannot easily escape because the density is very high. They remain trapped due to total internal reflection, inside what can be crudely thought of, as a neutrinosphere. For 10 MeV neutrinos a density of about 10^{12} gm/cc and above is sufficient for trapping. This gives us an estimate of the size of the neutrinosphere. The outer material, which is not in acoustic communication with the bouncing core, keeps falling in and the energy density at the boundary of the core and mantle keeps increasing until eventually the stellar matter bounces off the core creating a shock-wave which goes through the star and blasts off the outer envelope. This scenario where the shock-wave is the source of the explosion is known as the prompt explosion scenario. However, simulations suggest that the shock-wave loses a lot of its kinetic energy by dissociating the nuclei in the stellar matter, as it propagates outward. As a result, the shock-wave stops after about 100ms and cannot cause a successful explosion.

It is therefore conjectured that more energy must be deposited in the shock-wave while it moves outwards, for the explosion to be successful. This can be happen if neutrinos escape the neutrinosphere and deposit their energy behind

the shockwave. If enough energy is transferred to the shock-wave then the dying shock-wave can be revived and it can cause a successful explosion by blowing off the envelope of the star. This scenario is known as the delayed explosion scenario. The fact that almost all ($\sim 99\%$) of the energy of a SN goes out in neutrinos, makes this scenario quite plausible from energetic grounds. However, the exact mechanism of the explosion is not clear and the simulations do not always end in successful explosions, telling us that not everything is settled in our understanding of SN explosions. In fact simulations suggest that there are two shock-waves that are formed and that too can be understood in terms of explosion dynamics similar to but more detailed than the above treatment. Please refer to this review [66] for a detailed exposition of the explosion mechanism and this paper [16] for a more updated view of the subject.

3.1.2 Primary fluxes

Let us now focus on the primary fluxes of neutrinos that are expected from a SN. As the simplest approximation one can assume that the entire binding energy E_b of the star is converted to neutrinos. For a star with radius R and mass M the binding energy is,

$$E_b \approx \frac{3G_N M^2}{5R} = 1.60 \times 10^{53} \left(\frac{M}{M_\odot}\right)^2 \left(\frac{10\text{km}}{R}\right). \tag{3.1}$$

If one also assumes equipartition of energies among the different flavours, the total energy into each flavour is about $(1/6)E_b$. We know that the neutrinos are emitted from the surface of the neutrinosphere whose radius is about 10km. If we apply the virial theorem to estimate the average kinetic energy E_{kin} of the particles we have,

$$E_{kin} = \frac{G_N M m_N}{2R}. \tag{3.2}$$

This tells us that the neutrinos from a SN have energies of about 10MeV. The duration of neutrino emission is a multiple of the neutrino diffusion time-scale over the neutron star radius. This allows an estimate that neutrinos are emitted over a duration of order 1 second.

Neutrinos are emitted from a SN in roughly four distinct phases. In the phase when the star is collapsing, the flux is comparatively low but steeply rises

when the revived shock-wave travels through the neutrinosphere, breaking apart the nuclei. This suddenly releases a flavour-specific burst of ν_e for about a few milliseconds. This is known as the neutronisation burst phase. In the next phase, the mantle cools off by emitting neutrinos for about $0.5 - 1$ second. Finally the protoneutron star at the core cools by radiating away neutrinos for about $5 - 10$ seconds. This final phase is called the Kelvin-Helmholtz cooling phase. We will investigate the non-adiabatic matter effects that may be important in this final phase of neutrino emission.

There is a certain flavour dependence of the fluxes. In the central regions of the star neutrinos of all flavours are produced via pair production. The neutrinos interact with each other and the material and remain trapped. The ν_e and $\bar{\nu}_e$ are produced mainly by electron capture on nuclei. Since there are more neutrons than protons one gets more ν_e than $\bar{\nu}_e$. Equipartition theorem then tells us that the $\bar{\nu}_e$ have slightly higher energies. Among the neutrinos, the ν_μ and ν_τ decouple before the ν_e and therefore have a larger average energy.

The above general expectations are borne out by most elaborate simulations. However the detailed predictions are not identical. The exact energy spectrum, and luminosities of the neutrinos are not predicted unambiguously and merely relies on existing models.

While the spectra are time-dependent, the average energies do not depend strongly on time. The luminosity is very high in the early stages and decreases slowly with time. We will ignore the time-dependence of the primary spectra in the present analysis for simplicity. One should include effects of a time dependent spectra and density profile for a more complete treatment.

The primary fluxes of $\bar{\nu}_e$ and $\bar{\nu}_x$, denoted by $F^0_{\bar{\nu}_e}$ and $F^0_{\bar{\nu}_x}$ respectively, are parametrised by

$$F^0_{\nu_i} = \frac{\Phi_0}{E_0} \frac{(1+\alpha)^{1+\alpha}}{\Gamma(1+\alpha)} \left(\frac{E}{E_0}\right)^{\alpha} \exp\left[-(\alpha+1)\frac{E}{E_0}\right] \ . \tag{3.3}$$

For illustration, we choose two models of neutrino flux, the Garching model [67] that uses the parameters

$$\alpha_{\bar{\nu}_e} = \alpha_{\bar{\nu}_x} = 3 \ , \ E_0(\bar{\nu}_e) = 15MeV \ , \ E_0(\bar{\nu}_x) = 18MeV \ , \ \Phi_0(\bar{\nu}_e)/\Phi_0(\bar{\nu}_x) = 0.8 \ ,$$

and the Livermore model [68] that uses

$$\alpha_{\bar{\nu}_e} = \alpha_{\bar{\nu}_x} = 3\ ,\ E_0(\bar{\nu}_e) = 15MeV\ ,\ E_0(\bar{\nu}_x) = 24MeV\ ,\ \Phi_0(\bar{\nu}_e)/\Phi_0(\bar{\nu}_x) = 1.6\ .$$

The only experimental data that we can use to compare with the above predictions, comes from the supernova SN1987A that occurred in the Large Magellanic Cloud about 50 Kpc away. It resulted in 19 events at two detectors and does not constrain the simulations strongly. With planned detectors like Hyper-Kamiokande [69], a galactic SN could result in up to 100000 events in the first ten seconds of the explosion, which will allow us to learn a lot more about SN neutrino fluxes.

3.2 Phase effects in neutrino conversions in a supernova

Our approach is to take a given SN density profile [16] and primary spectra at a fixed time and numerically solve for the evolution of the neutrino wavefunctions through it. That allows us to calculate the conversion probabilities to be seen on earth. Then we convolve the conversion and survival probabilities with the primary fluxes and include effects like energy resolution of the detector, allowing us to calculate the expected signal with phase effects. We will end the chapter by enumerating what we could learn from such a signal and how we could extract information from it.

3.2.1 Observables for matter effects

To begin with, there are some simplifications to this reasonably complicated problem. The first simplification is that though we have to formally consider a three-neutrino mixing problem, it factorises into two simpler two-neutrino mixing problems. There are two independent Δm^2 values and that tells us that there will be two different densities at which the MSW resonance can occur. There is a significant hierarchy in the Δm^2 values and that assures us that the two resonances never happen together. This so called separation of H and L resonances [17] means that the three neutrino mass eigenstates travel independently

and if ever there is a jump probability between any two neutrinos, the third mass eigenstate is not involved. This immense simplification allows our two neutrino solutions to hold. The second simplification is that the L resonance that takes place in neutrinos is always adiabatic [19], whereas the jump probability P_H between the two mass eigenstates at the H resonance is equal to P_{ee} as computed in the previous chapter. The survival probability of ν_e after passing through both the H and L resonances is

$$p = P_H \sin^2\theta_\odot \quad \text{(NH)}, \quad p = \sin^2\theta_\odot \quad \text{(IH)} \tag{3.4}$$

where NH and IH stand for normal and inverted mass hierarchy respectively. Here $\theta_\odot$ is the solar mixing angle. Similarly, the survival probability of $\bar{\nu}_e$ after passing through both the H and L resonances is

$$\bar{p} = P_H \cos^2\theta_\odot \quad \text{(IH)}, \quad \bar{p} = \cos^2\theta_\odot \quad \text{(NH)}\ . \tag{3.5}$$

Clearly, since the phase effects appear through P_H, they will be visible only in ν_e for normal hierarchy and only in $\bar{\nu}_e$ for inverted hierarchy. There are important earth matter effects that have to be considered [70, 71] if these neutrinos pass through the earth but we will restrict our analysis to down-going events only.

In present and planned water Cherenkov [69] and scintillation [72] detectors, the main neutrino detection channel is the inverse beta decay reaction $\bar{\nu}_e p \rightarrow ne^+$ that allows the reconstruction of $\bar{\nu}_e$ energies. Therefore we consider only the $\bar{\nu}_e$ spectrum in our analysis. However an analogous analysis can be easily performed in the neutrino channel for a detector able to measure the ν_e spectrum, for example using liquid argon [73].

3.2.2 Results for a typical SN density profile

In order to illustrate the phase effects on p or $\bar{p}$, we consider a typical snapshot of the density profile of a SN during a shock-wave [16], as shown in figure 3.1. The resonance densities for $E = 5$ and 80 MeV are also shown taking $\Delta m^2 = 0.002\ eV^2$ and $\theta = 0.02$ rad $\approx 1.1°$. The forward shock F and the reverse shock R are sharp density discontinuities, the density change of a factor of two or more taking place over a distance of much less than a km. The density variation in the "contact

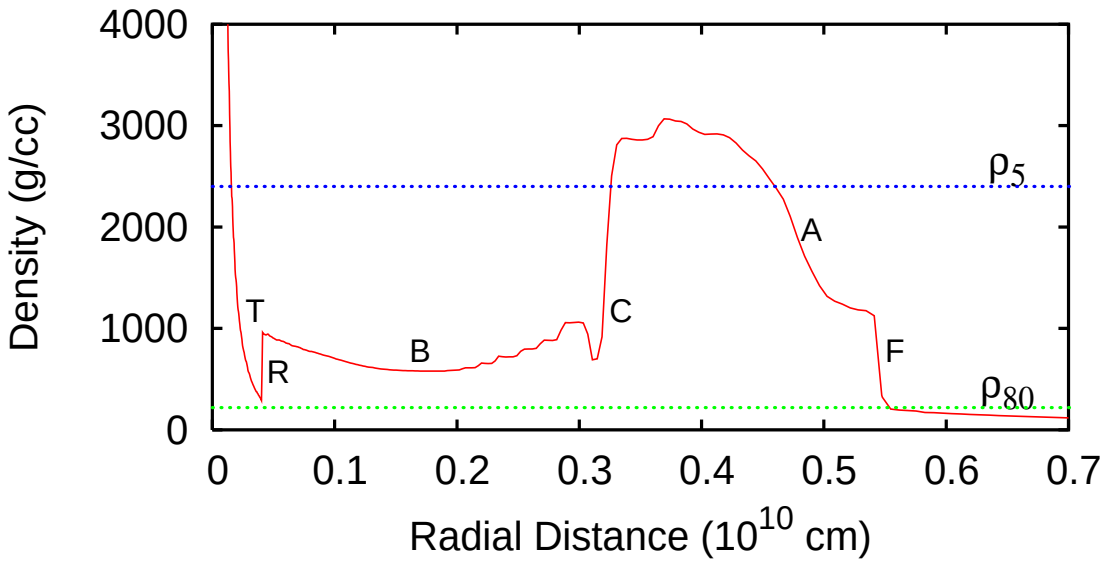

Figure 3.1: Snapshot of a shock-wave density profile at $t = 5$ sec.

discontinuity" C, which is the transition region between the shock-accelerated and neutrino-heated SN ejecta, takes place more slowly, over a distance of more than 100 km [16]. The mass accretion region A behind the forward shock-wave, and the low density bubble B have gradually changing densities. The region T is the tail of the shock-wave.

The neutrinos, while passing through these regions, may undergo multiple level crossings. The extent of flavour conversion in each region will depend on the value of θ_{13} and the steepness of the density profile in that region. It is found that for $\theta \sim 0.01$ rad or higher, the density variations in the mass accretion region A, the low density bubble B and the contact discontinuity C are too gradual for any non-adiabaticity. We therefore concentrate on the forward shock F, the reverse shock R and the tail T.

Figure 3.2 shows the value of $\bar{p}$ as a function of energy for $\theta = 0.02$ rad $\approx 1.1°$. The rapid oscillations correspond to the relative phase $\Phi_{RF}(\approx \Phi_{TF})$ that is accumulated by the mass eigenstates between resonances regions R and F (T and F). Such high frequency oscillations are virtually impossible to observe, given the practical limits on the energy resolutions of neutrino detectors.

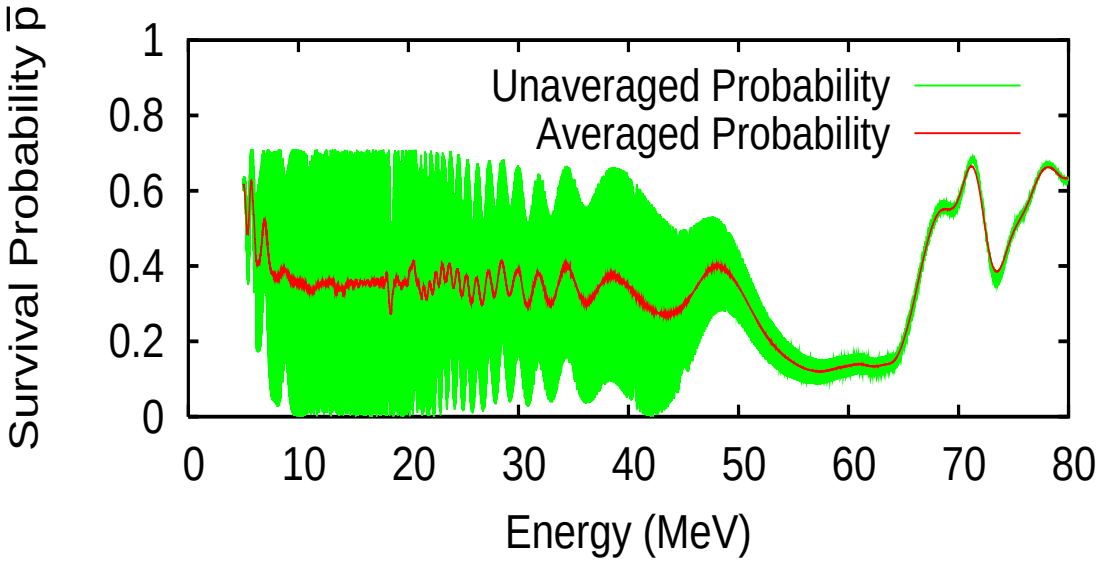

Figure 3.2: Survival probability $\bar{p}$ of $\bar{\nu}_e$ for inverted hierarchy with the density profile in figure 3.1. The "averaged probability" is obtained by taking a running average over the energy range corresponding to the typical energy resolution of a scintillation detector.

We average out these high frequency oscillations by taking a "running average" over the energy range corresponding to the typical energy resolution of a scintillation detector. The low frequency oscillations that survive are found to correspond to the relative phase Φ_{TR} accumulated by the mass eigenstates between resonances in regions T and R. Since these two resonances are closer compared to the resonance pairs R-F or T-F, the frequency of oscillations is smaller. The same oscillation pattern is observed if the survival probability is computed by assuming that the resonance in region F is completely adiabatic, which confirms that the pattern is indeed due to the level crossings in regions T and R. These low frequency oscillations may be observable at the neutrino detectors.

The second dip observed at $E \approx 70$–80 MeV is a part of the "double dip" feature pointed out in [16] that appears due to the presence of both the forward as well as the reverse shock. Note that $\bar{p}$ goes to $\cos^2\theta_\odot$ at both very low and very high energies, where P_H goes to unity. The oscillations in the low energy region ($E < 20$ MeV) are rapid, the fluctuations observed therein are in part due to numerical artifacts and details of the density profile and are not a robust feature.

In order to demonstrate the oscillation effects in the observed $\bar{\nu}_e$ flux at a neutrino detector, we plot in figure 3.3(a) the quantity

$$dN_{\bar{\nu}_e}/dE_{\bar{\nu}_e} = \sigma(E_{\bar{\nu}_e})F_{\bar{\nu}_e} = \sigma(E_{\bar{\nu}_e})[F^0_{\bar{\nu}_x} + \bar{p}(F^0_{\bar{\nu}_e} - F^0_{\bar{\nu}_x})] \tag{3.6}$$

as a function of the neutrino energy $E_{\bar{\nu}_e}$, where we have normalised the spectrum such that the total number of events is 10^5. Here we use the differential cross section as computed in [74] including the leading QED radiative corrections and final state interactions. It may be observed that the oscillation wavelengths in the energy range 30–60 MeV are $\approx$ 2–8 MeV. Moreover, the positions of the extrema are independent of the primary fluxes.

The observation of the oscillation pattern in $\bar{\nu}_e$ spectrum would imply the following:

- It confirms that the mass hierarchy is inverted (if the oscillations were in ν_e spectrum, the hierarchy would have been normal.)

- The time interval during which the oscillations appear tells the times at which the shock-wave was present in the region of densities 500–5000 g/cc.
- The mixing angle θ_{13} is nonzero. Indeed, $\sin^2\theta_{13} \gtrsim 10^{-5}$ for the oscillations to be observable.
- If θ_{13} has already been measured at reactor experiments, one can obtain constraints on the slopes of the features within the shock-wave profile. In particular, even though the forward and the reverse shock may be taken to be almost density discontinuities, the slope of the tail T needs to be steep enough to ensure that the resonance there is semi-adiabatic.
- With $\Delta m^2 = \Delta m^2_{\rm atm}$ known and θ_{13} small, the distance between consecutive maxima or minima of the oscillation pattern depends only on the density profile immediately behind the reverse shock. This could allow us to reconstruct the profile of the tail region.

However, the spectrum shown in figure 3.3(a) is not directly observable: one can only observe the energy spectrum of positrons produced by the inverse beta reaction. Assuming quasielastic scattering, the positron energy is given by [74]

$$E_e = \frac{(E_\nu - \delta)(1+\epsilon) + \epsilon\cos\vartheta\sqrt{(E_\nu-\delta)^2 - m_e^2\kappa}}{\kappa}, \quad p_e = \sqrt{E_e^2 - m_e^2} \qquad (3.7)$$

where ϑ is the angle of scattering, M_p the proton mass, $\epsilon \equiv E_{\bar\nu_e}/M_p$, and $\kappa \equiv (1+\epsilon)^2 - (\epsilon\cos\vartheta)^2$. For $E \approx 40$ MeV, we have $\epsilon \approx 1/25$, so that the positron energy is spread over a range of ≈ 4 MeV depending on the scattering angle. Given that the successive maxima of the oscillation pattern are separated by only about 2–8 MeV in this energy range, the oscillation pattern is significantly smeared out.

A further smearing of the oscillation pattern is caused by the finite energy resolution of the detector. The energy resolution of a water Cherenkov detector is typically $\Delta E_{\rm CH}({\rm MeV}) \approx 1.6\sqrt{E(10{\rm MeV})}$ and washes off the oscillations completely. For a scintillation detector, the resolution is much better, $\Delta E_{\rm SC}({\rm MeV}) \approx 0.2\sqrt{E(10{\rm MeV})}$.

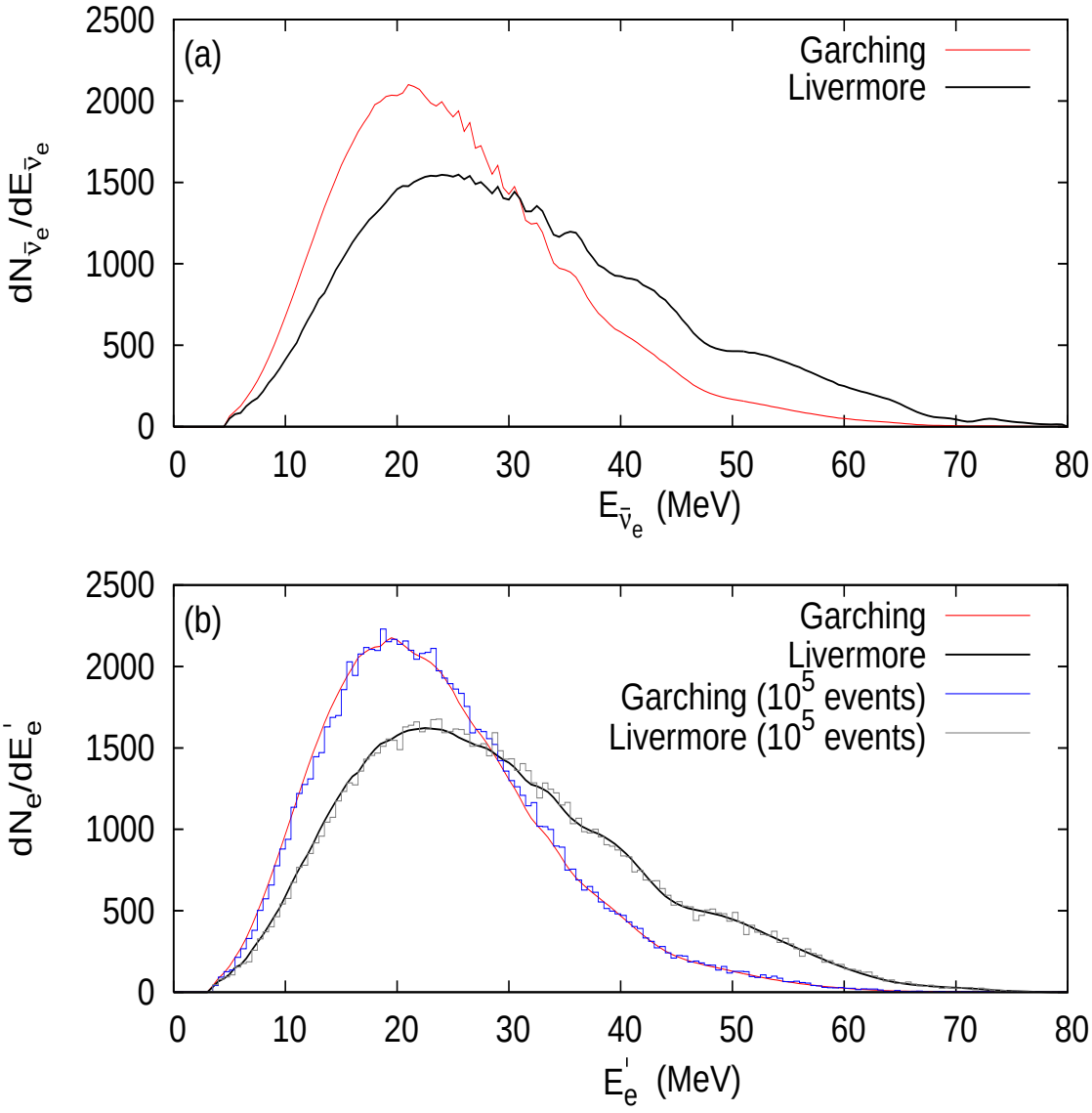

Figure 3.3: The upper figure (a) shows the oscillations in the energy spectra of the $\bar{\nu}_e$, if the $\bar{\nu}_e$ energy were accurately measurable, for the Garching and Livermore models. The bottom figure (b) shows the observed positron energy spectra in a scintillation detector. All the spectra are normalised so that the total number of events is 10^5. The figure (b) also shows the statistical fluctuations for 10^5 events with an energy binning of 0.5 MeV.

There is also the additional problem that the density profile itself changes with time. While in principle that should allow tracking the shape of the tail in time, the practical problem is that it severely limits statistics.

We show in figure 3.3(b) the spectrum of the observed positron energy E'_e after taking (3.7) into account and using the energy resolution of a scintillation detector. It is observed that one or two extrema at high energies ($E \approx$ 40–60 MeV) may still survive for the Livermore model where the spectrum extends to higher energies, but their clean identification would require $\sim 10^5$ events at a scintillation detector in a single time bin.

Figure 3.3(b) also shows the positron energy spectrum for 10^5 events, binned in 0.5 MeV energy intervals, which is approximately the energy resolution of a scintillation detector near $E = 40$ MeV.

The total number of events expected even at a future 50 kt scintillation detector is $\sim 10^4$ for a SN at a distance of 10 kpc [72]. Even with 1 sec time bins, the number of events in each bin will be $\sim 10^3$. This is a number too small for our purposes. Thus, the identification of the phase effects seems very unlikely, unless the SN is as close as a kpc.

The density profiles in the shock wave are quite uncertain, and one may expect that some possible profiles give rise to oscillations with larger amplitudes and wavelengths, which would be easier to observe. In general, larger amplitudes need a larger ratio $|A'(T)/A'(R)|$ [see (2.41) and (2.42)], whereas larger wavelengths need a sharp tail, i.e. a larger $|A'(T)|$. At the same time, the adiabaticity parameter at the two resonances has to be $0.1 \lesssim \gamma \lesssim 2$ for $E \approx 40$ MeV. However, we find that even with such finely tuned density profiles, the improvement in observability is not significant.

Chapter 4

Conclusions

Neutrino oscillations have provided us with the first glimpse of physics beyond the SM. The formalism that we have now, explains satisfactorily the solar and atmospheric neutrino deficits. It also explains the detailed signatures observed in numerous other experiments using reactor or accelerator neutrinos. The paradigm of massive neutrinos is thus now a part of the standard picture. The consolidation of this framework will involve precise measurement of the neutrino masses and the mixing angles. Numerous experiments with the above goal, are either already operational, or in a stage of development. We must reiterate at this stage that understanding of matter effects is crucial for many of these experiments. In particular, non-adiabatic matter effects may be important when neutrinos experience a sharp density discontinuity, as is the case for SN shockfronts and the core-mantle discontinuity in the earth. This was the primary reason for us to study matter effects on neutrino oscillations.

We have, in this thesis presented a technique to calculate neutrino conversion probabilities for arbitrary matter profiles using a perturbation theory in the relevant mixing angle, which needs to be small. Our method is specially useful whenever there is more than one non-adiabatic MSW resonance encountered by the neutrinos. An analytic understanding of the matter effects can be arrived at using our results, which is useful for the determination of oscillation parameters from the observed neutrino spectra.

We discuss the enhancement (or depletion) of neutrino conversion due to the presence of multiple non-adiabatic MSW resonances. We remark that there are

important interference effects in such a scenario, which depend on the adiabatic phase acquired by a neutrino between two resonances. This acquired phase depends on the energy of the neutrino and therefore the neutrino conversion is enhanced (or depleted) at certain energies. These phase effects are not neglible and cannot, in general, be ignored. We also show that the oscillatory pattern in the observed energy spectrum allows a reconstruction of the density profile in the region where the neutrinos undergo a resonance. We also show that in the event that the acquired phase changes too rapidly as a function of energy, the oscillations get averaged out and the result corresponds to ignoring the phase effects.

We have also applied our technique to a particular case where we expect important signatures of phase effects, i.e. to SN neutrinos. Neutrinos coming out of an exploding SN, experience multiple MSW resonances that are not adiabatic. We find that phase effects are present in the conversion probabilities and that they affect the observed spectrum. However, the oscillations in the spectrum do not seem possible to detect with present or planned detectors, given the limitations to their energy resolution. Nevertheless, we have mentioned the conclusions that can be drawn from an observation of the phase effects.

There are several limitations to our approach. Our method of calculating the wavefunctions perturbatively depend on knowing the density profile accurately. It might be interesting to what effect small fluctuations about the given profile have on the results. Our calculation also makes a saddle point approximation at the resonances. Clearly at certain energies it does not hold good anymore. Application of the our technique to some specific density profiles does bring about the existence of phase effects in principle. As far as SN neutrinos is concerned, we dont seem to get observable effect with density profiles that one gets from SN simulations. With some minor modifications the above profiles seem to produce larger phase effects, but probably still insufficient to be observed. We have not studied in depth, the effects of small fluctuations in the density profile. We have ignored earth matter effects in our treatment and also have not taken into account the time dependence of the neutrino signal. Some of these simplifications could be done away with to produce a more robust treatment.

It will be interesting to apply some of the ideas developed in this thesis, to a neutrino beam travelling through the earth and encountering the core-mantle density discontinuity. Whether the phase effects are sizable in this case and if so whether they will be observable. It is encouraging to note that the uncertainities in fluxes and the density profile will be much less in this case. The fact that the source luminosity will not depend drastically on time, will also allow for longer exposure time and better statistics. In the event that the phase effects are observable, it will tell us about the density profile at the core-mantle interface.

References

[1] K. S. Hirata *et al.* [Kamiokande-II Collaboration], Phys. Lett. B **280** (1992) 146. 2

[2] J. N. Bahcall and R. K. Ulrich, "Solar Models, Neutrino Experiments And Helioseismology," Rev. Mod. Phys. **60** (1988) 297. 2

[3] G. Altarelli and F. Feruglio, "Neutrino masses and mixings: A theoretical perspective," Phys. Rept. **320** (1999) 295. 2

[4] N. Cabibbo, "Unitary Symmetry And Leptonic Decays," Phys. Rev. Lett. **10** (1963) 531. 2

[5] M. Kobayashi and T. Maskawa, "CP Violation In The Renormalizable Theory Of Weak Interaction," Prog. Theor. Phys. **49** (1973) 652. 2

[6] B. Pontecorvo, Sov. Phys. JETP **26** (1968) 984 [Zh. Eksp. Teor. Fiz. **53** (1967) 1717]. 2, 13

[7] Z. Maki, M. Nakagawa and S. Sakata, Prog. Theor. Phys. **28** (1962) 870. 2

[8] L. Wolfenstein, "Neutrino Oscillations In Matter," Phys. Rev. D **17** (1978) 2369. 2, 16

[9] S. P. Mikheev and A. Y. Smirnov, "Resonant Amplification Of Neutrino Oscillations In Matter And Solar Neutrino Spectroscopy," Nuovo Cim. C **9** (1986) 17. 3, 17

[10] S. P. Mikheev and A. Y. Smirnov, "Resonance Enhancement Of Oscillations In Matter And Solar Neutrino Spectroscopy," Sov. J. Nucl. Phys. **42** (1985) 913 [Yad. Fiz. **42** (1985) 1441]. 3, 17

[11] S. J. Parke, "Nonadiabatic Level Crossing In Resonant Neutrino Oscillations," Phys. Rev. Lett. **57** (1986) 1275. 3

[12] A. Dighe, "Neutrino Physics-An Introduction", SERC School Lectures at Kanpur (2005). 3, 16

[13] R. N. Mohapatra and P. B. Pal, "Massive neutrinos in physics and astrophysics. Fourth edition," World Sci. Lect. Notes Phys. **72** (2004) 1. 3

[14] C. W. Kim and A. Pevsner, "Neutrinos in physics and astrophysics," Harwood Academic Publishers, 1993. 3

[15] M. C. Gonzalez-Garcia and Y. Nir, Rev. Mod. Phys. **75** (2003) 345 [hep-ph/0202058]. 3

[16] R. Tomas, M. Kachelriess, G. Raffelt, A. Dighe, H. T. Janka and L. Scheck, JCAP **0409** (2004) 015 [astro-ph/0407132]. 4, 36, 38, 39, 40, 42

[17] T. K. Kuo and J. T. Pantaleone, "Neutrino Oscillations In Matter," Rev. Mod. Phys. **61** (1989) 937. 4, 12, 38

[18] A. Dighe, "Supernova neutrinos: Production, propagation and oscillations," Nucl. Phys. Proc. Suppl. **143** (2005) 449 [hep-ph/0409268]. 4

[19] A. S. Dighe and A. Yu. Smirnov, "Identifying the neutrino mass spectrum from the neutrino burst from a supernova," Phys. Rev. D **62** (2000) 033007 [hep-ph/9907423]. 4, 39

[20] R. C. Schirato, G. M. Fuller, (. U. (. LANL), UCSD and LANL), "Connection between supernova shocks, flavor transformation, and the neutrino signal," [astro-ph/0205390]. 4, 9

[21] K. Takahashi, K. Sato, H. E. Dalhed and J. R. Wilson, "Shock propagation and neutrino oscillation in supernova," Astropart. Phys. **20** (2003) 189 [astro-ph/0212195]. 4, 9

[22] G. L. Fogli, E. Lisi, D. Montanino and A. Mirizzi, Phys. Rev. D **68** (2003) 033005 [hep-ph/0304056]. 4

[23] B. Dasgupta and A. Dighe, "Phase effects in neutrino conversions during a supernova shock wave," [hep-ph/0510219]. 4

[24] C. Kraus *et al.*, Eur. Phys. J. C **40** (2005) 447 [hep-ex/0412056]. 4

[25] D. N. Spergel *et al.*, [astro-ph/0603449]. 4, 5

[26] F. Reines, H. S. Gurr and H. W. Sobel, "Detection Of Anti-Electron-Neutrino E Scattering," Phys. Rev. Lett. **37** (1976) 315. 4

[27] G. Danby et al, "Observation Of High-Energy Neutrino Reactions And The Existence Of Two Kinds Of Neutrinos," Phys. Rev. Lett. 9 (1962) 36. 5

[28] K. Kodama *et al.* [DONUT Collaboration], "Observation of tau-neutrino interactions," Phys. Lett. B **504** (2001) 218 [hep-ex/0012035]. 5

[29] S. Eidelman *et al.* [Particle Data Group], "Review of particle physics," Phys. Lett. B **592** (2004) 1. 5

[30] T. D. Lee and C. N. Yang, "Question Of Parity Conservation In Weak Interactions," Phys. Rev. **104** (1956) 254. 5

[31] C. S. Wu, E. Ambler, R. W. Hayward, D. D. Hoppes and R. P. Hudson, "Experimental Test Of Parity Conservation In Beta Decay," Phys. Rev. **105** (1957) 1413. 5

[32] J. I. Friedman and V. L. Telegdi, "Nuclear Emulsion Evidence For Parity Nonconservation In The Decay Chain Pi+ Mu+ E+," Phys. Rev. **105** (1957) 1681. 5

[33] E. C. G. Sudarshan and R. e. Marshak, "Chirality Invariance And The Universal Fermi Interaction," Phys. Rev. **109** (1958) 1860. 5

[34] R. P. Feynman and M. Gell-Mann, Phys. Rev. **109** (1958) 193. 5

[35] J. N. Bahcall, A. M. Serenelli and S. Basu, "New solar opacities, abundances, helioseismology, and neutrino fluxes," Astrophys. J. **621** (2005) L85 [astro-ph/0412440]. 6, 7

[36] B. T. Cleveland *et al.*, "Measurement of the solar electron neutrino flux with the Homestake chlorine detector," Astrophys. J. **496**, 505 (1998). 6

[37] P. Anselmann *et al.* [GALLEX Collaboration], "Update of GALLEX solar neutrino results and implications," Nucl. Phys. Proc. Suppl. **38** (1995) 68. 6

[38] J. N. Abdurashitov *et al.* [SAGE Collaboration], "Measurement of the solar neutrino capture rate in SAGE," Nucl. Phys. Proc. Suppl. **118** (2003) 39. 6

[39] S. Fukuda *et al.* [Super-Kamiokande Collaboration], "Solar B-8 and he p neutrino measurements from 1258 days of Super-Kamiokande data," Phys. Rev. Lett. **86** (2001) 5651 [hep-ex/0103032]. 6, 21

[40] B. Aharmim *et al.* [SNO Collaboration], "Electron energy spectra, fluxes, and day-night asymmetries of B-8 solar neutrinos from the 391-day salt phase SNO data set," Phys. Rev. C **72** (2005) 055502 [nucl-ex/0502021]. 7, 21, 22

[41] G. Barr, Nucl. Phys. Proc. Suppl. **143** (2005) 89. 8

[42] Y. Ashie *et al.* [Super-Kamiokande Collaboration], "A measurement of atmospheric neutrino oscillation parameters by Super-Kamiokande I," Phys. Rev. D **71** (2005) 112005 [hep-ex/0501064]. 8, 15, 16

[43] T. Araki *et al.* [KamLAND Collaboration], "Measurement of neutrino oscillation with KamLAND: Evidence of spectral distortion," Phys. Rev. Lett. **94** (2005) 081801 [hep-ex/0406035]. 9, 22

[44] K. Hirata *et al.* [KAMIOKANDE-II Collaboration], "Observation Of A Neutrino Burst From The Supernova Sn1987a," Phys. Rev. Lett. **58** (1987) 1490. 10

[45] R. M. Bionta *et al.*, "Observation Of A Neutrino Burst In Coincidence With Supernova Sn1987a In The Large Magellanic Cloud," Phys. Rev. Lett. **58** (1987) 1494. 10

[46] L. E. Strigari, J. F. Beacom, T. P. Walker and P. Zhang, "The concordance cosmic star formation rate: Implications from and for the supernova neutrino and gamma ray backgrounds," JCAP **0504** (2005) 017 [astro-ph/0502150]. 10

[47] A. Aguilar *et al.* [LSND Collaboration], "Evidence for neutrino oscillations from the observation of anti-nu/e appearance in a anti-nu/mu beam," Phys. Rev. D **64** (2001) 112007 [hep-ex/0104049]. 10

[48] G. L. Fogli, E. Lisi, A. Marrone and A. Palazzo, "Global analysis of three-flavor neutrino masses and mixings," [hep-ph/0506083]. 10

[49] Visit the websites www.hep.anl.gov/ndk/hypertext/nuindustry.html and http://cupp.oulu.fi/neutrino to see a list of completed, running and proposed neutrino experiments. 10

[50] L. Stodolsky, "The unnecessary wavepacket," Phys. Rev. D **58** (1998) 036006 [hep-ph/9802387]. 13

[51] Y. Ashie *et al.* [Super-Kamiokande Collaboration], "Evidence for an oscillatory signature in atmospheric neutrino oscillation," Phys. Rev. Lett. **93** (2004) 101801 [hep-ex/0404034]. 16

[52] E. Aliu *et al.* [K2K Collaboration], "Evidence for muon neutrino oscillation in an accelerator-based experiment," Phys. Rev. Lett. **94** (2005) 081802 [hep-ex/0411038]. 16

[53] P. B. Pal and T. N. Pham, Phys. Rev. D **40** (1989) 259. 16

[54] D. Notzold and G. Raffelt, "Neutrino Dispersion At Finite Temperature And Density," Nucl. Phys. B **307** (1988) 924. 16

[55] J. F. Nieves, "Neutrinos In A Medium," Phys. Rev. D **40** (1989) 866. 16

[56] J. Linder, "Derivation of neutrino matter potentials induced by earth," [hep-ph/0504264]. 16

[57] T. K. Kuo and J. T. Pantaleone, "Nonadiabatic Neutrino Oscillations In Matter," Phys. Rev. D **39** (1989) 1930. 18, 20

[58] L. Landau, "A theory of energy transfer II," Phys. Z. Sowjetunion **2** (1932) 46. 19, 24

[59] C. Zener, "Nonadiabatic Crossing Of Energy Levels," Proc. Roy. Soc. Lond. A **137** (1932) 696. 19, 24

[60] M. Kachelriess and R. Tomas, "Non-adiabatic level crossing in (non-) resonant neutrino oscillations," Phys. Rev. D **64** (2001) 073002 [hep-ph/0104021]. 20

[61] P. C. de Holanda and A. Y. Smirnov, JCAP **0302** (2003) 001 [hep-ph/0212270]. 20

[62] S. Goswami, A. Bandyopadhyay and S. Choubey, "Global analysis of neutrino oscillation," Nucl. Phys. Proc. Suppl. **143** (2005) 121 [hep-ph/0409224]. 22

[63] A. B. Balantekin, S. H. Fricke and P. J. Hatchell, "Analytical And Semi-classical Aspects Of Matter Enhanced Neutrino Oscillations," Phys. Rev. D **38** (1988) 935. 23

[64] A. S. Dighe, Q. Y. Liu and A. Yu. Smirnov, "Coherence and the day-night asymmetry in the solar neutrino flux," [hep-ph/9903329]. 31

[65] Georg G. Raffelt "Stars as Laboratories for Fundamental Physics," University of Chicago Press, 1996. 35

[66] H. A. Bethe, "Supernova Mechanisms," Rev. Mod. Phys. **62** (1990) 801. 36

[67] R. Buras, H. -Th. Janka, M. T. Keil, G. G. Raffelt and M. Rampp, "Electron-neutrino pair annihilation: A new source for muon and tau neutrinos in supernovae," Astrophys. J. **587** (2003) 320 [astro-ph/0205006]. 37

[68] T. Totani, K. Sato, H. E. Dalhed and J. R. Wilson, "Future detection of supernova neutrino burst and explosion mechanism," Astrophys. J. **496** (1998) 216 [astro-ph/9710203]. 38

[69] K. Nakamura, "Hyper-Kamiokande: A next generation water Cherenkov detector," Int. J. Mod. Phys. A **18** (2003) 4053. 38, 39

[70] A. S. Dighe, M. T. Keil and G. G. Raffelt, "Identifying earth matter effects on supernova neutrinos at a single detector," J. Cosmol. Astropart. Phys. JCAP06 (2003) 006 [hep-ph/0304150]. 39

[71] A. S. Dighe, M. Kachelriess, G. G. Raffelt and R. Tomàs, "Signatures of supernova neutrino oscillations in the earth mantle and core," J. Cosmol. Astropart. Phys. JCAP01 (2004) 004 [hep-ph/0311172]. 39

[72] L. Oberauer, F. von Feilitzsch and W. Potzel, "A large liquid scintillator detector for low-energy neutrino astronomy," Nucl. Phys. Proc. Suppl. **138** (2005) 108. 39, 45

[73] A. Bueno, I. Gil-Botella and A. Rubbia, "Supernova neutrino detection in a liquid argon TPC," [hep-ph/0307222]. 39

[74] A. Strumia and F. Vissani, "Precise quasielastic neutrino nucleon cross section," Phys. Lett. B **564** (2003) 42 [astro-ph/0302055]. 42, 43